ACS OMEGA

http://pubs.acs.org/journal/acsodf

Article

Fine Migration Control in Sandstones: Surface Force Analysis and Application of DLVO Theory

Rizwan Muneer, M. Rehan Hashmet,* and Peyman Pourafshary

Cite This: *ACS Omega* 2020, 5, 31624–31639

Read Online

ACCESS | Metrics & More | Article Recommendations

ABSTRACT: Formation damage caused by fine migration and straining is a well-documented phenomenon in sandstone reservoirs. Fine migration and the associated permeability decline have been observed in various experimental studies, and this phenomenon has been broadly explained by the analysis of surface forces between fines and sand grains. The Derjaguin−Landau−Verwey−Overbeek (DLVO) theory is a useful tool to help understand and model the fine release, migration, and control phenomena within porous media by quantifying the total interaction energy of the fine−brine−rock (FBR) system. Fine migration is mainly caused by changes in the attractive and repulsive surface forces, which are triggered by mud invasion during drilling activity, the utilization of completion fluid, acidizing treatment, and water injection into the reservoir during secondary and tertiary recovery operations. Increasing pH and decreasing water salinity collectively affect the attractive and repulsive forces and, at a specific value of pH, and critical salt concentration (CSC), the total interaction energy of the FBR system (V_T) shifts from negative to positive, indicating the initiation of fine release. Maintaining the system pH, setting the salinity above the CSC, tuning the ionic composition of injected water, and using nanoparticles (NPs) are practical options to control fine migration. DLVO modeling elucidates the total interaction energy between fines and sand grains based on the calculation of surface forces of the system. In this context, zeta potential is an important indicator of an increase or decrease in repulsive forces. Using available data, two correlations have been developed to calculate the zeta potential for sandstone reservoirs in high- and low-salinity environments and validated with experimental values. Based on surface force analysis, the CSC is predicted by the DLVO model; it is in close agreement with the experimental value from the literature. The critical pH value is also estimated for alkaline flooding. Model results confirm that the application of NPs and the presence of divalent ions increase the attractive force and help to mitigate the fine migration problem. Hence, a new insight into the analysis of quantified surface forces is presented in current research work by the practical application of the DLVO theory to model fine migration initiation under the influence of injection water chemistry.

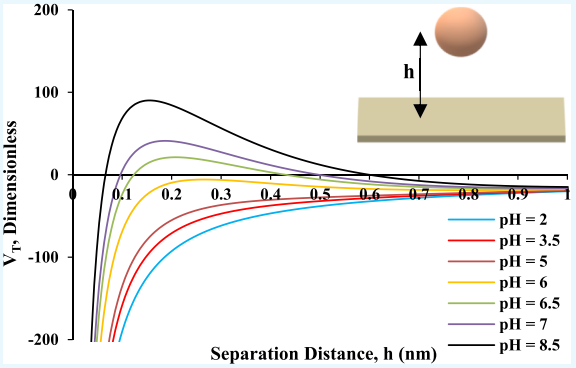

INTRODUCTION

The decrease in ionic strength (I_s) and change in ionic composition of formation water lead to fine migration and permeability reduction in subsurface porous and permeable sandstone reservoirs containing various types of clay minerals. Such minerals are present in the pore space as either agglomerate particles or as fine particles which cover the sand grains. Clay minerals are alumino-silicates with a very specific layered structure. The basic building blocks of clay minerals are layers of silica, alumina, and magnesia. There are major three types of clay minerals which include kaolinite, montmorillonite, and illite/mica.[1,2] Sandstones consist of a matrix of quartz grains enclosing an interconnected pore space. The nature of the depositional environment can lead to the presence of siliceous fines because of grain compaction and crushing because of applied stresses as well as fine deposition. These fines are generally held within the formation water film that surrounds the quartz grain in water-wet conditions.[3] Fine migration may happen in different types of natural and technical processes, such as water aquifer recharging by some external water source, underground formation water disposal, groundwater flows, and invasion of drilling muds, invasion of completion fluids, acidizing and waterflooding treatments, high rate oil and gas production and injection, and improper design of oil recovery processes with low-salinity water injection.[4−15]

Water injection operations into sandstone and carbonate reservoirs performed by reducing the salinity and tuning the ionic composition are a promising and evolving technology to

Received: August 16, 2020
Accepted: November 19, 2020
Published: December 2, 2020

maximize oil recovery, primarily by modifying the wettability of the crude−brine−rock system.[16−25] During the aforementioned process of waterflooding, the salinity, chemistry, and injection rate of injected brine play a vital role in altering the rock wettability and changing the surface forces between fines and sand grains in sandstone reservoirs, which affect the efficiency of the procedure.[17,24−30] Fine particles can detach, become suspended in the injected fluid, and form a colloidal system in the reservoir because of the alteration of attractive and repulsive surface forces; while they move with the injected fluid/brine, they may block the pore throats. This phenomenon is referred to as straining: it blocks already open pores and results in formation damage, with a substantial decline in formation permeability,[5,31−34] as shown in Figure 1.

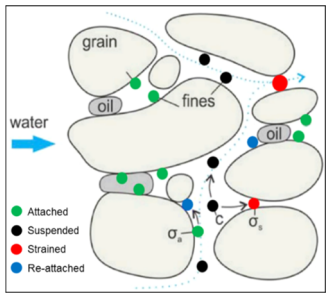

Figure 1. Migration of natural fine particles in the reservoir (reproduced with permission from *J. Nat. Gas Sci. Eng.* **2020**, *73*, 103047).[34]

Fine migration in sandstone reservoirs is supposed to be one of the possible mechanisms of enhanced oil recovery (EOR) in low-salinity projects. It provides better mobility control by plugging some of the pores, diverting flow toward unswept sections of the reservoir, and increasing the sweep efficiency, which eventually is favorable for incremental oil recovery.[2,27,28,35−42] As yet, fine-assisted oil recovery phenomenon is still not well understood and in-depth research on this issue is necessary to address the associated productivity and injectivity decline. On the other hand, fine migration has been reported by some researchers to have adverse effects on fluid productivity and injectivity, and their release, migration, and straining can significantly impair the hydraulic connectivity of the reservoir because they plug the actual path for fluid flow.[43−47]

Fine release and migration inside sandstone reservoirs are related to several factors such as the available concentration of fine particles, ionic composition, and salinity of injected water, pH, wettability, flow rate, and relative flow of different phases.[7,12,48,49] In some recent studies,[50−55] it has been found that CO_2 injection in sandstone can also lead to permeability reduction because of fine migration. Mineral dissolution caused by CO_2−brine−rock interaction could be the reason for fine particle generation in porous media and the related decline in CO_2 injectivity. Therefore, all these key factors must be considered to get an in-depth understanding of interactive forces between fine particles and sand grains in order to properly design a solution and mitigate the fine migration problem.

Various techniques have been developed and utilized to overcome the aforementioned problems and enhance oil recovery economically. Some examples include the utilization of clay stabilizers, matrix acidizing treatment,[56,57] adjusting the salinity, tuning the ionic composition, and changing the pH of the injected water.[30,58,59] The application of nanoparticles (NPs) is one of the emerging technologies used to fix the fine migration problem. NPs are extremely small particles; their size can vary between 1 and 100 nm, and they have a high surface-area-to-volume ratio because of their small size. NPs can change the surface properties of the materials to which they are adsorbed. A single type of NPs [in the form of nanofluids (NFs)], a combination of more than one type of NP (hybrid case), and also NPs and surfactants in combination are being used to reduce formation damage and enhance oil production.[60−65] NPs alter surface forces and potential as they are adsorbed on the rock. Several types of NPs with different chemical natures and distinct properties have been used to control fines migration; they include magnesium oxide (MgO),[61,66−68] silicon oxide (SiO_2),[60,69] and aluminum oxide (Al_2O_3).[65,69−71]

In the past, Martin[72] performed many waterflooding experiments on sandstone cores and observed that a decrease in injected water salinity resulted in additional oil recovery, accompanied by a decrease in core permeability because of clay swelling. Later, Khilar and Fogler[73] found that when injected fluid salinity falls below a critical salt concentration (CSC), fines are released and migration starts within porous media. Fine migration and subsequent permeability reduction were also confirmed by experimental research.[7,27,35,36,50,74−76] Kumar et al.[22] and Mansouri et al.[60] used scanning electron microscopy (SEM), the field emission SEM, and atomic force microscopy to visually show the mobilization of mixed-wet kaolinite particles with high-resolution images.

Attractive forces are responsible for retaining fines on the rock surface, whereas repulsive forces try to detach fines and promote migration. The Derjaguin−Landau−Verwey−Overbeek (DLVO) model incorporates surface forces and calculates the total interaction energy for the system, which is either positive or negative based on the contribution of each energy component.

In this paper, surface forces are quantified, and the DLVO model is used to predict the CSC for NaCl and to estimate a critical pH value for alkaline flooding. The model confirms that NPs increase the attractive energy and help fixate fines on sand grains. Furthermore, this tool has estimated an even lower CSC if there are divalent ions in the solution, which suggests the idea of tuning/adjusting the ion composition of injection water to avoid fine migration. Two correlations for the zeta potential calculation have also been developed and validated using further modeling. Therefore, the present study concludes that the analysis of quantified surface forces combined with DLVO modeling is a powerful tool to predict and control fine migration in porous media, and further research on the sensitivity of important parameters can improve the results.

FINE−BRINE−ROCK SYSTEM

The detachment of fine particles from the sand grain surface is the initial step in the process of fine migration in sandstones. A comprehensive understanding of this detachment process is necessary to analyze conditions for the migration and the resultant formation damage. Generally, two types of forces are responsible for the detachment and mobilization of fine particles. These forces are classified as colloidal forces and hydrodynamic forces. Colloidal forces are electrostatic in nature, and they are further divided into two types, which are London−van der Waals attractive forces and electrical double-layer repulsive forces between particles and surfaces. The hydrodynamic forces are mainly related to the flow of permeating fluid through porous media. Synthetic fines and silica glass beads have

https://dx.doi.org/10.1021/acsomega.0c03943
ACS Omega 2020, 5, 31624−31639

been used in numerous studies,[60,65−67,69,71,77] to mimic sandstone reservoirs with fine particles, as shown in Figure 2,

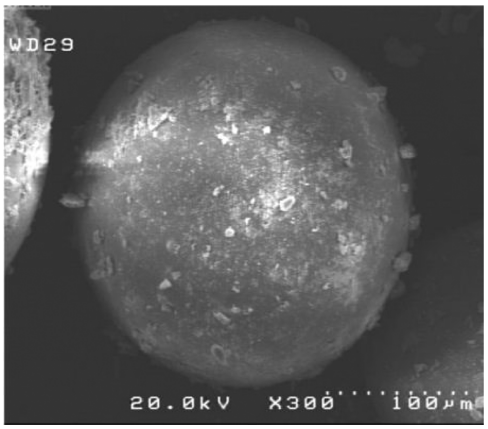

Figure 2. Adsorbed fines on the surface of a glass bead (reproduced with permission from *Colloids Surf., A* **2013,** *436,* 803−814).[65]

because they are spherical. However, kaolinite in sandstone reservoirs has a platelet structure with a finite thickness, while natural sand and glass beads both have infinite thicknesses (IT) as compared to fine particle size. Based on the aforementioned configuration of synthetic/natural fines and sand/glass beads, generally, there are different electrostatic energies for two different systems: the sphere−IT plate and the kaolinite platelet−IT plate.

An analysis of a single fine particle of presumably spherical shape on a sand grain surface had been performed to describe the conditions required for the detachment of fine from a flat surface.[78−81] Figure 3 describes the sphere−IT plate model

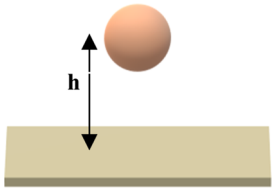

Figure 3. Spherical fine on sand grain surface.

designed to mimic a spherical fine particle attached to the pore/rock grain through which a high-salinity permeating liquid is flowing. However, Figure 4 demonstrates a kaolinite platelets−IT plate configuration, where small kaolinite platelets are present on a sandstone grain. Most of these platelets are in the form of clusters and can move together based on attractive forces between individual plates. Similar kaolinite platelet configurations have also been found in other sources.[82−87]

The separation distance (h) between a fine particle and the pore surface in Figure 3 is quite small (usually on the order of 10^{-1} nm), and additionally, these fine particles are subjected to the hydrodynamic forces of the flowing liquid during production and injection processes. There are different energy contributions from colloidal and hydrodynamic forces, and the total energy of all interactions between a fine particle and the pore/grain surface must be determined precisely in the DLVO model to incorporate the effects of attractive and repulsive forces. If the net interaction energy of the system comes out to be positive, it means repulsive forces have dominance over the attractive

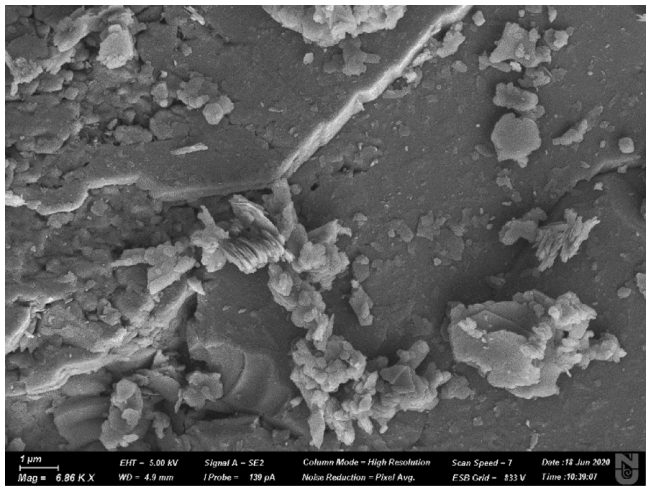

Figure 4. Kaolinite platelets−IT plate configuration.

forces; as a result, fines will be detached from the surface, and migration will start in the porous medium.

During early research studies and to date, a single fine particle of spherical shape on a sand grain flat surface (sphere−plate model) has been extensively used for the calculation of DLVO interactions because of the simplicity of the approach.[33,65,67,71,77,88−92] A few researchers have utilized a plate−plate model for the quantification of interaction energies.[93,94] The single sphere model can be accurately used for synthetic fines and glass bead configurations, but when it comes to natural kaolinite and sand grain configurations, it can provide erroneous results because natural kaolinite has a platelet structure and must be modeled with a kaolinite platelets−IT plate model. In some studies during the last few years,[31,32,95−99] clustered fine particles' detachment and combined movement were assumed instead of a single fine particle model. Recently, Chequer et al.[90] used this new idea to show that the single-colloid single-surface system is not an accurate representation of colloidal behavior in porous media and significantly underestimates the critical velocity of the fluid to initiate the fine migration. Experimental results were in close agreement with the clustered fines model.

DLVO THEORY

The well-known DLVO theory was established by Derjaguin, Landau, Verwey, and Overbeek.[100−102] It describes the V_T of the system incorporating attractive and repulsive forces because of the van der Waals attractive potential (V_{LVW}), electric double-layer (EDL) potential (V_{EDL}), and Born repulsive potential (V_{BR}). This theory assumes that the V_{LVW}, V_{EDL}, and V_{BR} potentials are independent of each other and therefore can be added for the particle−plate system, using either a sphere−plate or plate−plate model configuration, to quantify total interaction energy at each interacting distance. The DLVO-based V_T of the system composed of a fine particle and a pore surface is presented as eq 1.

$$V_T = V_{LVW} + V_{EDL} + V_{BR} \quad (1)$$

Generally, the DLVO theory provides good estimates for the surface−surface forces with a separation distance of around 5 nm, provided that all the important parameters, such as the particle size, I_s, Hamaker constant (A_H), and zeta potential (ζ), are accurately and precisely measured. The total energy of a

https://dx.doi.org/10.1021/acsomega.0c03943
ACS Omega 2020, 5, 31624−31639

specific system can range from positive (repulsive) to negative (attractive) depending on the individual contributions of the attractive and repulsive forces.

Application of DLVO Theory in the Petroleum Industry. The DLVO theory has been widely used in the petroleum industry to quantify surface forces between fines and sand grains during NF injection scenarios, disjoining pressure estimation, and polymer and surfactant adsorption on the rock surface. Quantification of DLVO-based interactions has been reported to be in close agreement with experimental results. Habibi et al.[71] utilized NPs in synthetic cores to mitigate the fine migration problem, computed total interactions, and found that MgO NPs improved the attractive forces between fines and the grain surface. Arab and Pourafshary[65] performed several experiments on glass beads to mitigate the fine migration issue, accompanied by low-salinity flooding. They used five different types of NPs to control fine migration and found that ZnO and γ-Al_2O_3 NPs were the best at this task. In addition to experimental results, they also measured the zeta potentials of the system before and after the application of NFs and applied a DLVO sphere−IT plate model to calculate interactive energy. The total energy was attractive after the application of NPs as compared to the nontreated case. Arab et al.[67] performed experiments using SiO_2 and MgO NPs in the preflush mode and found that 0.03% MgO NPs performed the best among all scenarios. They confirmed their experimental findings with the DLVO theory by calculating the total interaction potential between the rock and fine particles.

Assef et al.[66] demonstrated their work to mitigate colloidal particle movement in porous media by using MgO NPs, and 97% retention of fines was observed. They utilized the extended DLVO (X-DLVO) theory by incorporating the effect of acid−base energy and neglecting the hydrodynamic forces and quantified the total interaction energy of the system. Zou et al.[103] applied the X-DLVO theory to investigate the adsorption of anionic polyacrylamide onto coal and kaolinite particles. Based on the results, they observed that the V_T between kaolinite and coal particles was repulsive after the adsorption of the polymer on coal particles, which proves the effectiveness of the mechanism of coal purification.

QUANTIFICATION OF INTERACTION ENERGIES

London−Van Der Waals (V_{LVW}) Interaction Energy. In particle physics, there exists an attractive force between similar particles/plates when they are infinitesimally close to each other. A German-American physicist, Fritz London, published the first satisfactory microscopic theory of dipole−dipole dispersion forces.[104] This attractive force is a distance-dependent force between molecules, atoms, and particles and does not have any association with any type of ionic or covalent bonds. It decays slowly and acts at a distance less than 10 nm. The main cause of this electrostatic force is the presence of permanent and oscillating dipoles of atoms.[12] These forces are weak chemical forces, but still play a critical role when colloidal particles are infinitesimally close to each other in a solution. Based on the sphere−IT plate model, London−van der Waals energy (V_{LVW}) is presented in two forms, in eqs 2,[79] and 3.[105]

$$V_{LVW} = -\frac{A_H a_p}{12h} \quad (2)$$

$$V_{LVW} = -\frac{A_H}{6}\left[\frac{2(1+H)}{H(2+H)} + \ln\left(\frac{H}{2+H}\right)\right] \quad (3)$$

Chequer et al.[90] presented a new model based on the clustered fine sphere−IT plate model, as shown in eq 4.

$$V_{LVW} = -n\frac{A_H}{6\sqrt{2}\,a_p}\left(\frac{a_p}{h}\right)^{5/2} \quad (4)$$

On the other hand, a separate model for kaolinite platelets−IT-plate configuration has been presented by Gregory et al.,[79] as shown in eq 5.

$$V_{LVW} = -\frac{A_H}{12\pi h^2} \quad (5)$$

The negative sign of V_{LVW} demonstrates the attractive nature of this potential.

EDL (V_{EDL}) Interaction Energy. When charged colloidal particles (fines) are immersed in an electrolyte solution of specific ionic strength, mobile ions from the electrolyte solution form an ionic film around the particles.[102] Based on the positive or negative charge of a particle, oppositely charged ions from the surrounding electrolyte solution are attracted and form an ionic layer over the charged particle called a compact layer (stern layer), which is moved with the particle. The excess charge on the compact layer is balanced by the oppositely charged ions from the electrolyte solution forming another layer, which is called the diffuse layer (slipping plane). In the diffuse layer, ions are not tightly bound to each other and are free to move to and from the electrolyte solution. These two layers are electrostatic, and their combined effect is called the EDL, as shown in Figure 5.[106]

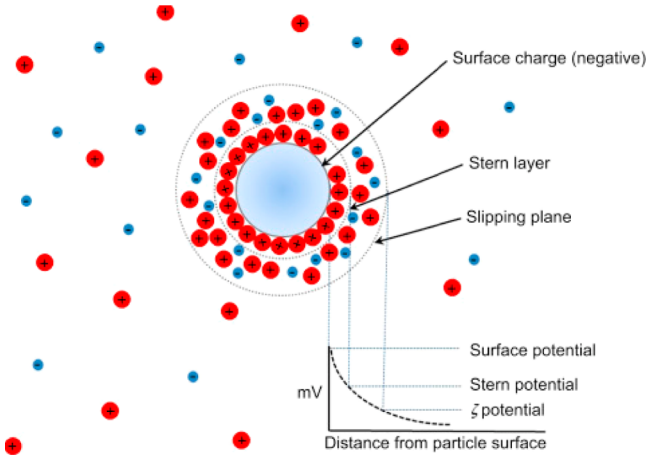

Figure 5. Compact and diffuse EDLs and corresponding zeta potential (reproduced with permission from Elsevier: Amsterdam, The Netherlands, **1995**; pp 113−156).[106]

The potential difference between these two layers is called zeta potential and is denoted by ζ. Zeta potential provides the closest surface potential estimate and is used in the quantification of the EDL interaction energy. Zeta potential is not directly measured and is obtained by applying an electric field across the dispersion: this process is called electrophoresis.[107,108] Particles within the dispersion with a specific zeta potential value move toward the electrode of opposite charge with a velocity proportional to the magnitude of the zeta potential. At lower ion strength, such as in the low-salinity

https://dx.doi.org/10.1021/acsomega.0c03943
ACS Omega 2020, 5, 31624−31639

injection condition, EDLs that have already formed around the sand grain surface and the fine particles expand and overlap, which leads to a repulsive interaction energy (V_{EDL}). High repulsive force may detach the fine particles from the sand grain surface. The repulsive force is higher at a lower solution salinity.

Regarding the formulation of V_{EDL}, the simplest case of sphere−plate geometry is used, as shown in Figure 3. For the boundary conditions, the rock and fine particle surfaces both may have a constant surface potential or constant charge, or one of the surfaces may maintain its charge density constant while the other surface possesses a constant potential (mixed case). Generally, fine migration can be modeled with a constant potential case because zeta potential is easy to measure as compared to surface charge. V_{EDL} can be calculated by different formulae, such as eqs 6, 7,[109] or 8,[80] for the sphere−IT plate model.

$$V_{EDL} = \left(\frac{\epsilon a_p}{4}\right)\left[2\Psi_1\Psi_2 \ln\left(\frac{1 + e^{-kh}}{1 - e^{-kh}}\right) + (\Psi_1^2 + \Psi_2^2)\ln(1 - e^{-2kh})\right] \quad (6)$$

$$V_{EDL} = \left(\frac{\epsilon a_p}{4}\right)\left[2\zeta^2 \ln\left(\frac{1 + e^{-kh}}{1 - e^{-kh}}\right) + (2\zeta^2)\ln(1 - e^{-2kh})\right] \quad (7)$$

$$V_{EDL} = 2\pi\varepsilon_m\varepsilon_0 a_p\zeta^2 \cdot \ln(1 + e^{-h/k^{-1}}) \quad (8)$$

Equation 6 is valid for potentials less than 60 mV, when the double-layer thickness is less than the fine particle size, which is true in most scenarios of fine migration in sandstone porous media. Ψ_1 and Ψ_2 are the surface and compact layer potentials, respectively, and can be replaced by the measured value of the zeta potential (ζ-potential) to develop eq 7. Chequer et al.[90] presented a new model to calculate V_{EDL} based on the clustered fines sphere−IT plate model, as shown in eq 9.

$$V_{EDL} = -n160.4\varepsilon_m\varepsilon_{0k}(ka_p)^2\left(\frac{k_BT}{ze}\right)^2\gamma_s\gamma_g e^{-kh} \quad (9)$$

For V_{EDL} calculations based on the kaolinite platelets−IT-plate model, Gregory[110] presented a different model, as shown in eq 10.

$$V_{EDL} = \frac{64n_\infty k_B T}{k}\gamma_s\gamma_g e^{-kh} \quad (10)$$

Born Repulsion (V_{BR}) Interaction Energy. In a colloidal system, when particles approach and are about to contact each other, a short-range repulsive potential called the Born repulsion potential (V_{BR}) is generated because their electron clouds overlap. This potential is quite sensitive to the structure of surfaces in contact and permeating liquid. Formulations to quantify the Born repulsion potential for the previously described sphere−IT-plate system have been presented by Ruckenstein et al. and Schumacher et al.[111,112] in eq 11 and Mahmood et al.[81] in eq 12.

$$V_{BR} = \frac{A_H}{7560}\left(\frac{\sigma}{a_p}\right)\left[\frac{8 + H}{(2 + H)^7} + \frac{6 - H}{H^7}\right] \quad (11)$$

$$V_{BR} = \frac{A_H a_p \sigma^6}{1260h^7} \quad (12)$$

For clustered fine movement in the porous medium, Chequer et al.[90] presented a new model to calculate V_{BR}, as shown in eq 13.

$$V_{BR} = -n\frac{A_H a_p^2 \sigma^6}{45h^9} \quad (13)$$

A separate model for the natural kaolinite platelets−IT-plate configuration has been presented by Mahmood et al.[81] as eq 14.

$$V_{BR} = \frac{A_H\sigma^6}{360\pi h^8} \quad (14)$$

To compute Born repulsion accurately for the fines−rock−fluids system configuration, A_H and σ (atomic collision diameter, nm) must be known precisely. An average value used for σ in the calculation of V_{BR} is around 0.5 nm. Generally, V_{BR} has a very small impact on the V_T and can be neglected in comparison to other electrostatic potentials (V_{LVW} and V_{EDL}) if the separation distance is greater than 1 nm.

RESULTS AND DISCUSSION

The EDL expands because of alteration in the pH and ionic strength of the solution, which affects the repulsive force. In this section, we study the effect of these parameters on the total force and fine migration. As mentioned before, the application of NPs increases attractive energy by changing the surface potential to control fine migration, which is also investigated, and results are shown in this section using the DLVO approach.

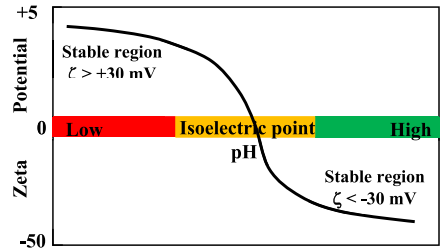

Figure 6. Change in zeta potential with pH of the solution (reproduced with permission from Woodhead Publishing, 2016; pp 299−325).[114]

Table 1. Zeta Potential Data Based on pH of the System

ionic strength	pH	ζ-potential (mV)	source
2 M (8 wt % NaCl + 2 wt % $CaCl_2$)	2	−7	Singh and Mohanty[115]
	3.5	−11	
	5	−16	
	6	−22.5	
	6.5	−26	
	7	−28	
	8.5	−32	

pH of Solution. The pH of colloidal dispersions is one of the most important factors that affect the repulsive force, and it is indicated by the change in the zeta potential of the system. Zeta potential is generally positive at low pH values (acidic region), and with increasing pH, it becomes negative because of the presence of excess OH^{-1}. There is a specific pH, where the zeta

https://dx.doi.org/10.1021/acsomega.0c03943
ACS Omega 2020, 5, 31624−31639

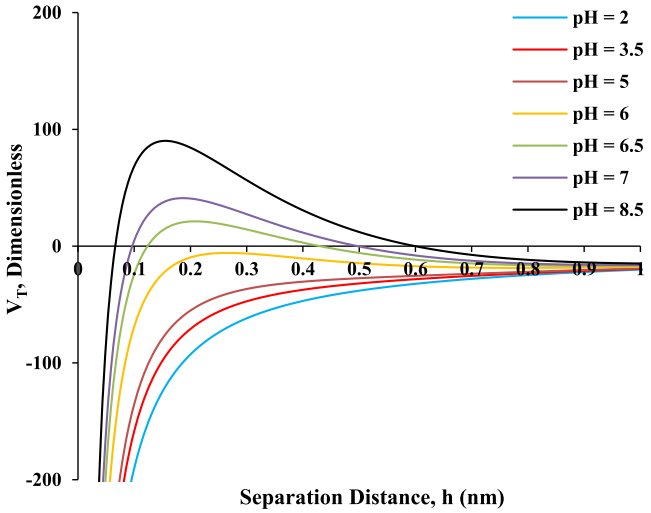

Figure 7. DLVO interactions and pH sensitivity analysis.

Table 2. Effect of Ionic Strength on EDL Thickness

$$k = \sqrt{\frac{\epsilon k_B T}{2N_A e^2 I_s}}$$

NaCl I_s at 298 K (M)	(nm)	ζ-potential (mV)[90]
0.6	0.4	−17.9
0.4	0.5	−21.3
0.2	0.7	−24.3
0.1	1	−30.5
0.05	1.4	−33.7
0.025	2	−34.0
0.01	3	−34.3

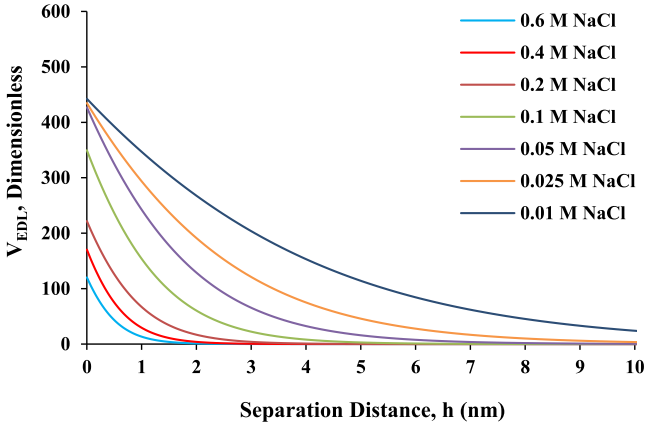

Figure 8. Effect of ionic strength on the EDL repulsion.

potential becomes zero, which is called the point of zero charge (PZC) or the isoelectric point (IEP), as shown in Figure 6. For a pH higher than the PZC, the surface charge becomes negative, which means a repulsive force that leads to the separation of fines. NPs can shift the PZC by changing the surface forces, so they can be used to control the repulsive force and the detachment of fines. The PZC for SiO_2 NPs is around pH = 2.5−3. For alumina, it lies between 7.5 and 9, and for MgO, it is around 12−13.[113] Hence, for highly alkaline conditions, the application of MgO NPs prevents fine detachment even at high pH values.

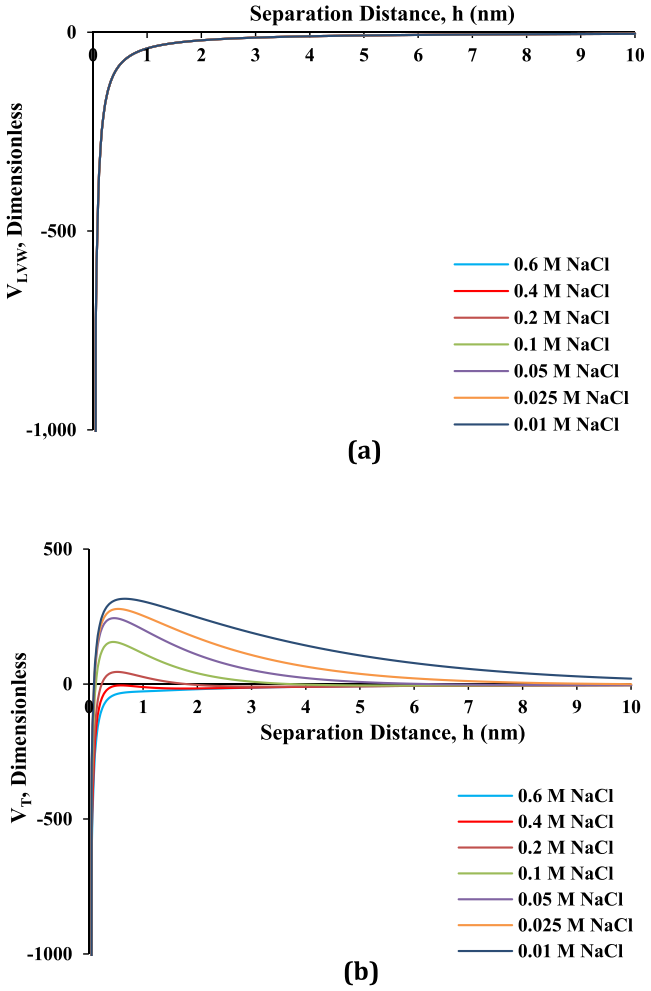

Figure 9. Effect of ionic strength on (a) attractive force and (b) total interaction energy.

Table 3. Zeta Potential Data for Analysis

salt	I_s (M)	ζ-potential (mV)	source
NaCl	0.3	−16	Chequer et al.[90]
	0.25	−18	
	0.2	−19	
	0.1	−23	
	0.02	−24.3	Assef et al.[66]
$CaCl_2$	0.02	−8.3	
$MgCl_2$	0.02	−6.09	

Table 4. Constants

parameter	symbol	value
fine particle radius	a_p	5×10^{-7} m
fluid temperature	T	297.15 K
pH of solution	pH	7
Boltzmann constant	k_B	1.38×10^{-23} J K^{-1}
Hamaker constant	A_H	3×10^{-21} J
permittivity of free space	e_o	8.85×10^{-12} C^2 J^{-1} m^{-1}
electron charge	e	1.6×10^{-19} C
Avogadro's number	N_A	6.02×10^{23} mol^{-1}
pi	π	3.1416
atomic collision diameter	σ	0.5 nm

https://dx.doi.org/10.1021/acsomega.0c03943
ACS Omega 2020, 5, 31624−31639

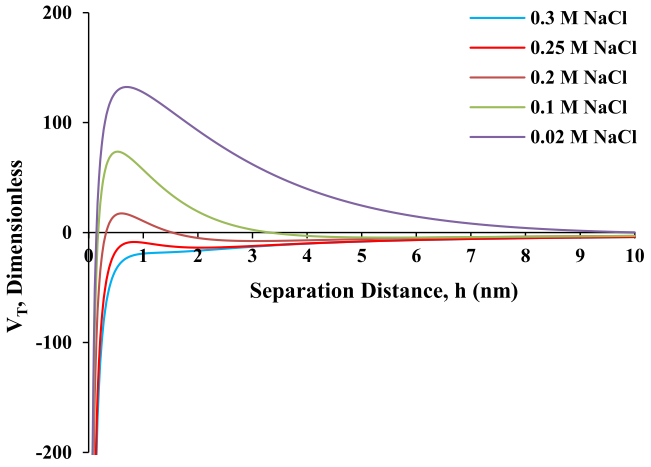

Figure 10. Prediction of CSC through DLVO interactions.

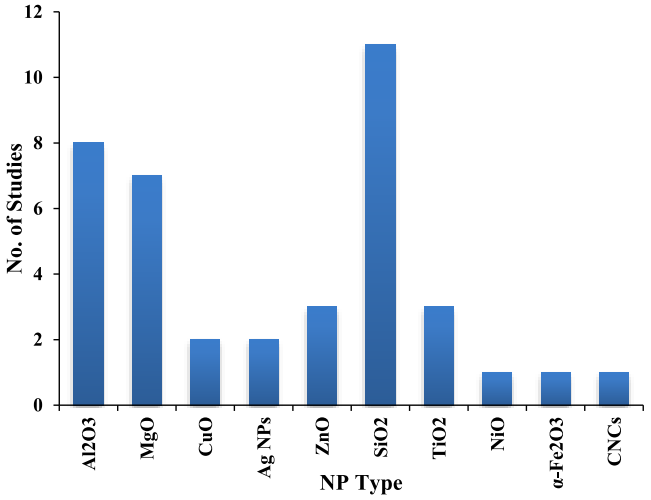

Figure 11. Different NP utilization in no. of studies.

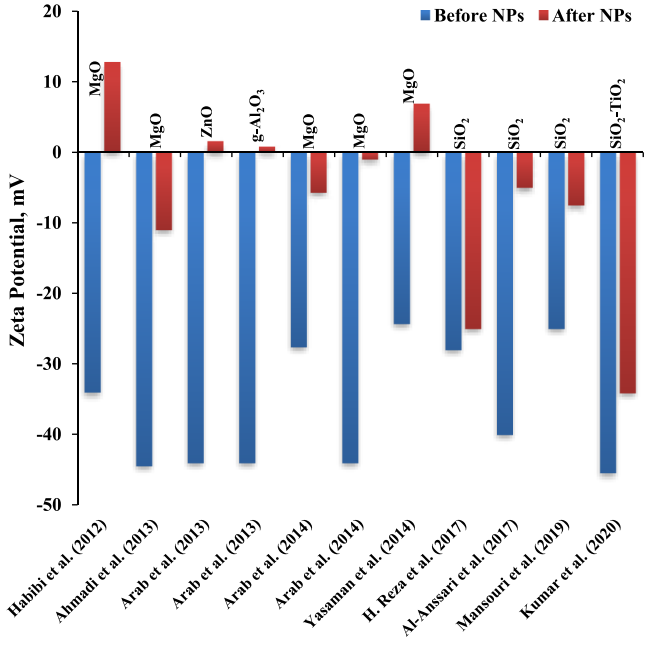

Figure 12. Change in zeta potential by the application of NPs.

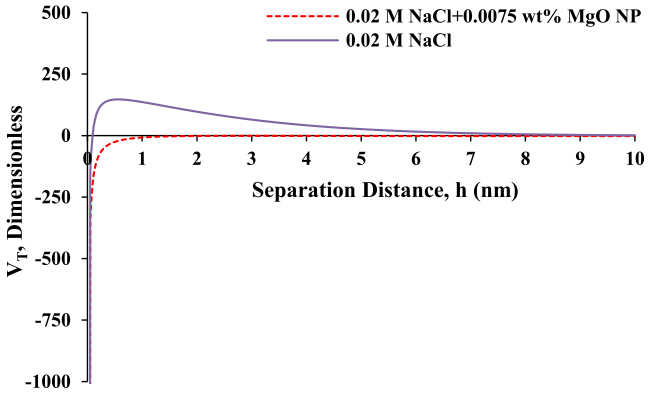

Figure 13. DLVO interactions for MgO NPs in NaCl solution.

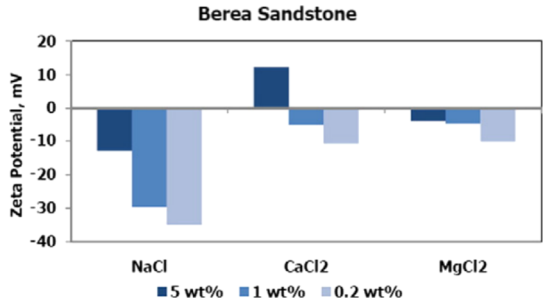

Figure 14. Monovalent and divalent ions effect on ζ-potential (reproduced with permission from *J. Mol. Liq.* **2016,** *221,* 658−665).[118]

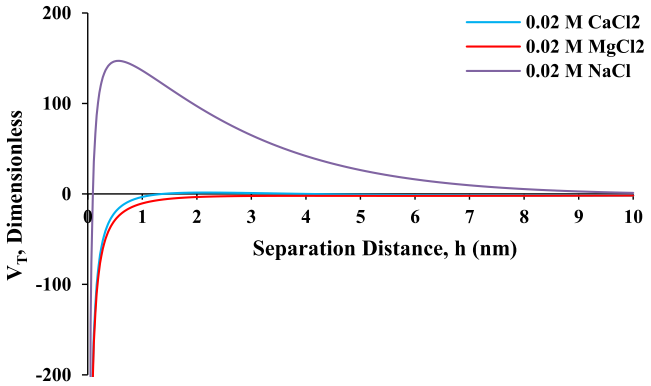

Figure 15. Effect of divalent ions on DLVO interactions.

pH Sensitivity Analysis Based on the DLVO Model. During alkaline flooding EOR, the alkali generates in situ surfactants that reduce the oil−water interfacial tension to maximize oil recovery. However, alkaline flooding in sandstones may cause fine migration problem because of the change in surface potential caused by an alteration in pH. As the pH of the system increases during alkaline flooding, the repulsive force between fine particles and sand grains increases, and the corresponding zeta potential decreases (becomes more negative) because of excess OH^{-1} in the system. This mechanism results in fine detachment and migration during alkaline flooding. The changes in zeta potential caused by increasing the pH of a high-salinity system, composed of a 2 M solution of 8 wt % NaCl with 2 wt % $CaCl_2$ and crushed sandstone grains with kaolinite particles, were measured and shown in Table 1. The DLVO model is used to calculate total energy for the case shown in this table and analyze the effect of pH values ranging from 2 to 8.5, as shown in Figure 7. Surface

https://dx.doi.org/10.1021/acsomega.0c03943
ACS Omega 2020, 5, 31624−31639

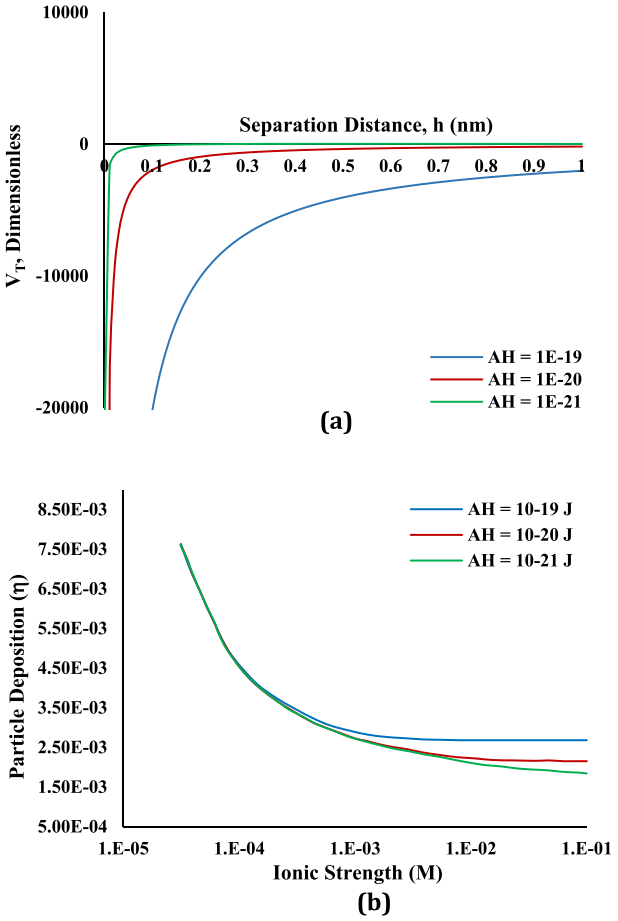

Figure 16. Effect of Hamaker constant on (a) DLVO interaction energy and (b) particle deposition (reproduced with permission from Elsevier, **1995;** pp 113−156).[124]

forces have been quantified, and the DLVO model has been applied to determine a critical pH value above which fine migration may begin.

Table 6. Validation of Zeta Potential Correlations

		zeta potential (mV)		
data source	I_s (M)	lab	model	error (%)
Fogden et al.[129]	0.0171	−39.0	−37.1	4.8
Lebedeva and Fogden[130]	0.075	−36.6	−31.6	13.8
	0.75	−14.7	−14.8	0.7
Hussain et al.[36]	0.05	−30.0	−34.0	13.2
	0.25	−30.0	−27.6	7.9
	0.5	−20.0	−21.2	6.1
Xie et al.[118]	0.1711	−30.0	−29.7	1.1
Shehata Nasr-El-Din[119]	0.8557	−12.0	−12.1	0.8
	0.1	−31.0	−31.2	0.6
	0.0856	−32.0	−30.5	4.6
	0.034	−35.0	−35.5	1.5
Walker and Glover[131]	0.5	−21.0	−21.2	1.1
	0.7	−16.0	−16.1	0.6
Chequer et al.[90]	0.025	−34.0	−36.4	7.0
	0.05	−34.0	−34.0	0.1
	0.2	−24.0	−28.9	20.5
	0.4	−21.0	−23.8	13.3

The critical pH value to initiate fine migration is between 6 and 6.5 for this case. Thus, maintaining the system pH below 6 can prevent fine migration. This calculation shows that the application of alkaline flooding leads to fine migration because in alkaline flooding the pH will be more than 7.

Ionic Strength (I_s). The ionic strength of the solution affects the expansion and thickness of the EDL, which further affects the repulsive force and total energy of the system. The higher the ionic strength of the solution, the more compressed the EDL becomes. For the quantification of EDL repulsion, the ionic strength and the corresponding experimental zeta potential data have been taken from research work by Chequer et al.[90] The effect of decreasing the ionic strength on the Debye length (k), which is an indicator of EDL thickness, is shown in Table 2. As the solution salinity decreases, EDLs around the fine particles and the sand grains both expand simultaneously, generating

Table 5. Hamaker Constant Data

author	year	base liquid	pH	T (°C)	system	A_H (J)	experimental/theoretical
El-Monier and Nasr-El-Din[93]	2011	distilled water	12	149	kaolinite−quartz	1.61×10^{-20}	experimental
Habibi et al.[71]	2012	water	7	25	glass beads−water	6×10^{-21}	theoretical
El Badawy et al.[122]	2012	0.03 M NaCl	7		metallic NPs	6.04×10^{-20}	experimental
Arab and Pourafshary[65]	2013	water	7	25	glass beads−water	6×10^{-21}	theoretical
Arab et al.[65]	2013	0.03 M NaCl	6.9	25	glass beads−brine	1×10^{-21}	theoretical
Arab and Pourafshary[67]	2014	water	7	25	glass beads−water	6×10^{-21}	theoretical
Habibi et al.[88]	2014	0.03 M NaCl	6.5−7	25	sand−NaCl	1×10^{-20}	theoretical
Xie et al.[25]	2014	0.2 wt % NaCl	8.1	65	oil/silica in water	8×10^{-21}	theoretical
Yang et al.[89]	2016	water		25	kaolinite and quartz	2×10^{-20}	theoretical
Mahani et al.[21]	2017	0.035 M diluted sea water	7	25	limestone−brine	1×10^{-19}	theoretical
Hasanneja et al.[77]	2017	0.3 M NaCl	7	25	glass beads−brine	1×10^{-20}	theoretical
Xie et al.[125]	2018	NaCl, $MgCl_2$ and $CaCl_2$	4−10	25	shale-oil	0.81×10^{-20}	theoretical
Huang et al.[91]	2018	2 wt % KCl	7	25	coal−brine	4.62×10^{-20}	theoretical
Sanaei et al.[94]	2019	0.01 M NaCl	7	25	carbonate−brine	1.3×10^{-20}	theoretical
Chequer et al.[90]	2019	0.6 M NaCl	7	25	kaolinite−sand	1.49×10^{-20}	experimental
Takeya et al.[23]	2020	0.1 M ALSW	7	25	calcite−brine	6.6×10^{-21}	theoretical
Tangparitkul et al.[33]	2020	0.0005 M NaCl brine			clay−sand	2×10^{-21}	theoretical
Gomez-Flores et al.[92]	2020	0.001 M NaCl	7	25	silica−brine	3.91×10^{-21}	theoretical
Peng et al.[123]	2020	0.007 M SDS and 0.0005 M NaCl		25	surfactant−water	5.2×10^{-20}	experimental

https://dx.doi.org/10.1021/acsomega.0c03943
ACS Omega 2020, 5, 31624−31639

Table 7. Zeta Potential Data in the Presence of NPs

authors	year	NP type	NP size (nm)	NP conc.	base liquid	pH	T (°C)	environment	ζ-potential (mV) before	ζ-potential (mV) after	apparatus/ method
Rouxel et al.[132]	2011	Al_2O_3	13	0.03 wt %	DI water	7.2	25	water	–	34	Zetasizer
Priya et al.[133]	2012	CuO	40–60	0.016 vol %	DI water	12	28–55	water	–	30	Zetasizer
El Badawy et al.[122]	2012	H_2–Ag	13	3 vol %	0.03 M NaCl	7		saline	–	−22	Zetasizer
Suganthi and Rajan[134]	2012	ZnO	30–45	1 vol %	DI water	–	25	water	–	49.9	Zetasizer
Habibi et al.[71]	2012	MgO	63	–	DI water	7	40	glass beads	–	−5.68	Zetasizer
			63	0.03 wt %	0.3 M NaCl	7	25	Berea sand		−7	Zetasizer
			63	0.1 wt %	DI water	7	25	glass beads	−34	12.8	Zetasizer
Ahmadi et al.[69]	2013	MgO	63	0.1 wt %	DI water	7	25	glass beads	−44.4	−11	Zetasizer
		SiO_2	48	0.1 wt %	DI water	7	25	glass beads		−22.5	Zetasizer
		Al_2O_3	43	0.1 wt %	DI water	7	25	glass beads		−28.4	Zetasizer
Arab and Pourafshary[65]	2013	ZnO	30	0.03 wt %	DI water	7	25	glass beads	−44	1.57	Zetasizer
		γ-Al_2O_3	20	0.03 wt %	DI water	7	25	glass beads	−44	0.82	Zetasizer
Arab et al.[67]	2014	MgO	20	0.03 wt %	0.03 M NaCl	6.9	25	glass beads	−27.6	−5.7	Zetasizer
		MgO	20	0.03 wt %	DI water	7	25	glass beads	−44	−1	Zetasizer
Assef et al.[66]	2014	MgO	20	0.0075 wt %	0.02 NaCl	7	25	glass beads	−24.3	6.9	Zetasizer
Bayat et al.[135]	2015	Al_2O_3	40	0.005 wt %	DI water	6.4	26	water	–	19.1	ζ analyzer
		TiO_2	30	0.005 wt %	DI water	6.4	26	water	–	9.1	ζ analyzer
		SiO_2	20	0.005 wt %	DI water	6.4	26	water	–	−28.1	ζ analyzer
Alomair et al.[64]	2015	TiO_2	50	0.1 wt %	30000 ppm brine	5.9	40	Berea sand	–	−13.2	Zetasizer
		SiO_2	15	0.1 wt %	30000 ppm brine	5.9	40	Berea sand	–	−28.3	Zetasizer
		Al_2O_3	40	0.1 wt %	30000 ppm brine	5.9	40	Berea sand	–	25.3	Zetasizer
		NiO	50	0.1 wt %	30000 ppm brine	5.9	40	Berea sand	–	−23.4	Zetasizer
Sabiha et al.[136]	2016	SWCNT	2500 L	0.1 vol %	DI water	–	25	water		−53.1	Zetasizer
Adil et al.[137]	2016	ZnO	55	0.1 wt %	30000 ppm NaCl	9	95	saline		−20	Zetasizer
Hasannejad et al.[77]	2017	SiO_2	145	0.1 wt %	0.3 M NaCl	7	25	glass beads	−28	−25	Zetasizer
Lee et al.[138]	2017	SiO_2	37	6.72 wt %	4.5 M $NaCl/CaCl_2$	8	25	saline		−24	Zetasizer
Al-Anssari et al.[117]	2017	SiO_2	10	0.1 wt %	1 wt % NaCl	6.3	–	saline	−40	−5	Zetasizer
Abdelfatah et al.[139]	2017	SiO_2	10	–	–	6	25	–	–	−22	–
Skoglund et al.[140]	2017	Ag NPs	9	–	DI water	–	25	water	–	−44	Zetasizer
Choudhary et al.[141]	2017	γ-Al_2O_3	20	0.1 wt %	DI water	7.6	–	water	–	36.7	Zetasizer
Upendar et al.[142]	2018	α-Fe_2O_3	20	0.05 wt %	0.001 M NaCl	6.5	25	saline	–	9.7	EFM
Kuang et al.[143]	2018	Al_2O_3	50	0.1 wt %	0.001 M NaCl	7	25	saline	–	39	ζ analyzer
Mansouri et al.[60]	2019	SiO_2	15	0.1 wt %	0.03 M NaCl	5.9	25	glass beads	−25	−7.5	Zetasizer
Ma et al.[144]	2019	SiO_2-g-SPMA	100	0.5 wt %	5.4 M NaCl + $CaCl_2$	11	170	saline	–	54	Zetasizer
Siddiqui et al.[62,145]	2019	Cu–Al_2O_3	270	0.01 wt %	DI water	7	23	water	–	48.15	ζ analyzer
Aramendiz and Imqam[146]	2019	SiO_2	20	0.75 wt %	DI water	9.5	25	water base mud	–	−34.66	ζ analyzer
Kumar et al.	2020	SiO_2–TiO_2	15, 20	0.4, 0.05 wt %	DI water	7	90	water	−45.4	−34.1	Zetasizer
Wang et al.[147]	2020	CNCs	70	0.25 wt %	0.175 M NaCl	7	21	saline	–	−60	Zetasizer

more repulsion between the fines and the sand grains. Consequently, detachment of the fines occurs.

The low zeta potential confirms the high repulsive force in these conditions. Figure 8 demonstrates the increase in repulsive force when the ionic strength is reduced from a high-salinity (0.6 M) to low-salinity environment (0.01 M). However, a decrease in brine salinity does not affect van der Waals attraction at any molarity, as depicted by the DLVO model in Figure 9a. Both energy contributions result in the total energy for the system incorporating constant attraction and variable repulsion at different salinities, indicating a critical salinity from 0.2 to 0.4 M, below which we may have fine detachment, as shown in Figure 9b.

For systems containing silica glass beads, fines, and 0.02 M NaCl, $CaCl_2$, and $MgCl_2$ solutions, zeta potentials have been measured by Assef et al.[66] Data for 0.3–0.1 M NaCl have been measured by Chequer et al., as shown in Table 3. We applied the DLVO approach to estimate the CSC value for these cases. Calculations of attractive and repulsive forces have been made for salinities from 0.3 to 0.02 M, and the results are shown in terms of the dimensionless V_T of the system. Data used in the model are given in Table 4.

https://dx.doi.org/10.1021/acsomega.0c03943
ACS Omega 2020, 5, 31624–31639

Table 8. Zeta Potential Data without NPs

authors	year	base liquid	salinity	pH	T (°C)	environment	ζ (mV)	apparatus/method
Yousef et al.[148]	2012	seawater	600 ppm	7−8	60	carbonate	−13	Zetasizer
Nasralla and Nasr-El-Din[128]	2012	NaCl brine	0.2 wt %	7.7	25	Berea SS	−35	phase-analysis light-scattering PALS
Hussain et al.[36]	2013	NaCl brine	0.5 M	–	25	sand	−20	–
Chen et al.[149]	2014	formation water	14000 ppm	8	25	limestone	−15	phase-analysis light-scattering PALS
Xie et al.[25]	2014	0.2 wt % NaCl	0.2 wt %	8.1	65	sandstone	−23.7	Zetasizer
Xie et al.[118]	2016	NaCl brine	0.2 wt %	–	25	sandstone	−33	–
Yao et al.[150]	2016	distilled water	0	9.2	25	quartz	−23	Zetasizer
Mahani et al.[21]	2017	diluted seawater	0.035 M	7	25	limestone	−11	Zetasizer
Huang et al.[91]	2018	KCl	2 wt %	7	25	coal−brine	−12.61	micro-electrophoresis
Sanaei et al.[94]	2019	NaCl brine	0.01 M	7	25	carbonate	−50	–
Chequer et al.[90]	2019	NaCl brine	0.6 M	7	25	sand	−20	Zetasizer
Takeya et al.[20]	2019	NaCl brine	0.7 M	7.2	50	crude oil	−23	ζ analyzer
Alghamdi et al.[151]	2020	smart water	5761 ppm	7.4	–	carbonate	−8	Smoluchowski equation
Ruan et al.[152]	2020	0.1 M KCl	0.1 M	7	30	clay−brine	4.9	Zetasizer
Takeya et al.[23]	2020	ALSW	0.1 M	7	25	calcite−brine	−3.72	Zetasizer
Tangparitkul et al.[33]	2020	NaCl brine	0.000513 M	–	–	clay−sand	−50	Zetasizer
Gomez-Flores et al.[92]	2020	NaCl brine	0.001 M	7	25	silica−brine	−39	–
Peng et al.[123]	2020	7 mM SDS and 0.5 m NaCl brine	–	–	25	surfactant−water	−80	–

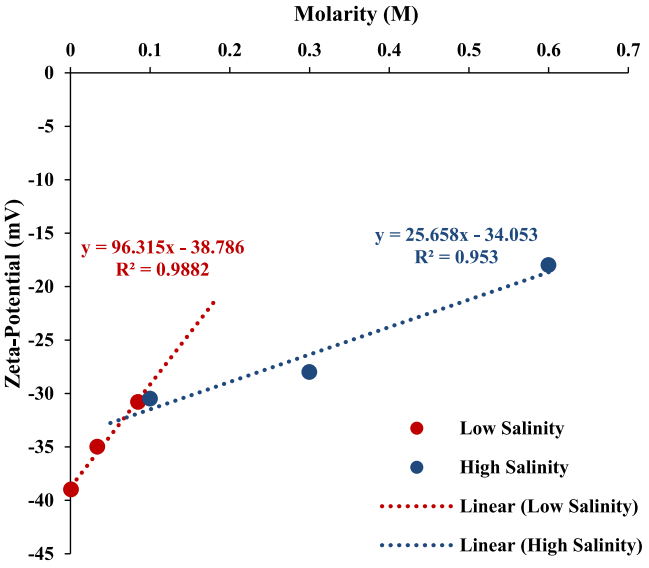

Figure 17. Zeta potential correlations for sandstone.

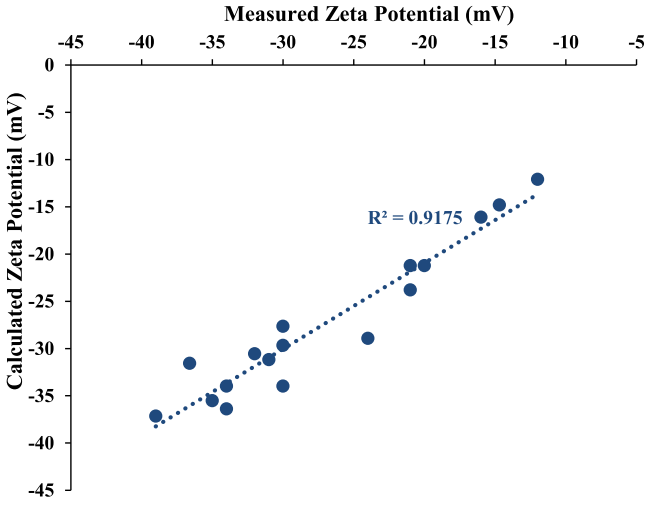

Figure 18. Close agreement between measured and calculated zeta potentials.

Figure 10 shows the effect of changing the salinity from 0.3 to 0.02 M NaCl solutions containing silica glass beads and fine particles to mimic a sandstone formation. The total DLVO energy for each scenario has been calculated using the sphere−IT plate DLVO model. As shown in Figure 10, total interaction energy is attractive for the high-salinity case because of the weak EDL repulsion. As the salinity is gradually decreased from 0.3 to 0.2 M, total system energy shifts from negative to positive, indicating that the EDLs have expanded and overlapped, causing an increase in repulsive forces (which dominated the attractive forces) under low-salinity conditions. It is observed from the DLVO model calculation that the CSC for the NaCl system is in the range of 0.2−0.25 M, which is in close agreement with the experimental value for the NaCl solution.[12,60]

Nanoparticles. Data concerning various NPs used in different studies, which were performed for fine fixation, wettability modification, interfacial tension (IFT) reduction, drilling mud preparation, and stable NFs formulation, have been collected, and the results have been presented in Figure 11.

It is observed that the maximum number of studies are performed using SiO_2 NPs because of their high stability, low toxicity, resistance to pH changes, and easy availability.[116] MgO and Al_2O_3 NPs are next on the list and have been utilized in several studies to mitigate fine release, the migration issue, and IFT reduction, respectively. NPs are used to overcome the fine migration problem in sandstone reservoirs by changing the surface forces, which can be observed by an alteration in zeta potential values before and after the adsorption of NPs onto rock/grain surfaces. Figure 12 presents zeta potential values of glass beads before and after the application of different NPs in low-salinity conditions.[60,63,65−67,69,71,77,117] Figure 12 shows that MgO NPs are the best at changing the surface energy and increasing zeta potential. In a few research studies, ZnO, TiO_2, and NiO NPs, and combinations of more than one NP, have been used in the form of NFs. Future research will benefit most

https://dx.doi.org/10.1021/acsomega.0c03943
ACS Omega 2020, 5, 31624−31639

from using different types of single and hybrid NFs. In an experimental study, Assef et al.[66] used MgO NPs to mitigate the adverse effects of fine migration that were noticed under low-salinity flow conditions (0.02 M NaCl).

They observed experimentally that the application of only 0.0075 wt % MgO NPs retained around 97% of in situ fine particles even in highly alkaline conditions of pH = 9.2. Retention of fine particles was attributed to increasing attractive forces between fines and glass beads in the presence of MgO NPs. To validate the experimental results, we applied the DLVO theory to quantify the total energy of the system, which is presented in Figure 13. Surface force quantification and analysis showed that the application of NPs increased the attractive forces between fines and grains and consequently the V_T of the system decreased, indicating a shift from repulsion to attraction.

Divalent Ions. The presence of divalent ions (Ca^{2+}, Mg^{2+}) in the solution is beneficial and can suppress the EDL thickness, resulting in reduced repulsive force as compared to monovalent ions (Na^+) for the same salinity. Xie et al.[118] performed experimental research and measured zeta potentials for a solution containing crushed sand particles in the presence of monovalent (Na^+) and divalent ions (Ca^{2+}, Mg^{2+}) separately. They observed that divalent ions suppressed the EDL which was formed around the sand grain and hence resulted in reduced repulsion, which is indicated by low zeta potential (absolute value), as shown in Figure 14.

Similar results for zeta potential data were observed in the studies performed by Shehata and Nasr-El-Din[119] and Gulgonul[120] on sandstone and natural hydrophobic Teflon, respectively, in the presence of monovalent and divalent ions (Ca^{2+}, Mg^{2+}). Assef et al.[66] also utilized $CaCl_2$ and $MgCl_2$ solutions and performed similar experiments. Quantification of surface forces has been done, and the DLVO model has been applied. Figure 15 depicts the relative comparison of V_T for monovalent and divalent ions in the electrolyte solution. The presence of divalent ions reduces the repulsive force and suppresses the expansion of the EDL even under low-salinity conditions because of their high valence charges. Divalent ions in the solution can help to design a lower value of the CSC, which means that low-salinity flooding benefits can be achieved without fine migration in sandstone reservoirs by tuning the composition of the injection brine.

Interactive Parameters for the FBR System. Van der Waals particle−particle attraction is produced when particles/molecules come close to each other in a medium. The Hamaker constant is a coefficient that relates this interactive energy among particles, whereas zeta potential (ζ) is a measure of the surface charge of the particles and an indicator of increase and decrease of the repulsive force. The following section discusses these parameters in detail.

Hamaker Constant (A_H). Hamaker constant is dependent on the integrated system of the fine particle, its shape, pore surface, aqueous medium type, and salinity, and crude oil properties.[80] The Hamaker constant is determined experimentally with great caution based on the specific system configuration. The typical values for A_H are found in the range of 10^{-21} to 10^{-19} J. These experimental values are in close agreement with the theoretical calculations of Israelachvili.[80,121] Equation 15 is used to calculate this constant using experimental data.

$$A_H = \frac{3}{4}k_B T\left(\frac{\varepsilon_1 - \varepsilon_3}{\varepsilon_1 + \varepsilon_3}\right)\left(\frac{\varepsilon_2 - \varepsilon_3}{\varepsilon_2 + \varepsilon_3}\right) + \frac{3h_p\nu_e}{8\sqrt{2}}(\eta_1^2 - \eta_3^2)$$
$$(\eta_1^2 - \eta_3^2) \Big/ \{(\eta_1^2 + \eta_3^2)^{1/2}(\eta_2^2 + \eta_3^2)^{1/2}$$
$$[(\eta_1^2 + \eta_3^2)^{1/2} + (\eta_2^2 + \eta_3^2)^{1/2}]\} \quad (15)$$

ε is the static dielectric constant, η is a refractive index, the subscripts 1, 2, and 3 refer to particles, grains, and water/brine, respectively, h_p is the Planck constant (6.62×10^{-34} J s), and ν_e is a constant value of electronic adsorption frequency equal to 3×10^{-15} s^{-1}. Table 5 presents studies where Hamaker constants were calculated and a few studies where experimental approaches have been used to measure A_H based on the system's actual configuration.[90,93,122,123] A sensitivity analysis for A_H has been performed and total interaction energy has been quantified in Figure 16. A high Hamaker constant leads to more attraction, whereas its low value is related to reduced attraction, as demonstrated by the DLVO model in Figure 16a. Also, particle deposition onto a rock's surface is affected by the Hamaker constant of the interactive system. Elimelech et al.[124] found that at low salinity, the range of EDL is much higher than that of van der Waals attraction, and the rate of particle deposition is mainly controlled by double-layer repulsive energy.

However, at high-salinity, van der Waals attractive forces are more effective, and as a result, the rate of particle deposition is controlled by A_H. Figure 16b illustrates the effect of different A_H values on particle deposition at different salinities. More particle deposition is observed because the repulsion is reduced at high A_H in a high-salinity environment. Hence, it is recommended that the experimental value of Hamaker constant be used in modeling, for the fine particle, rock grain, temperature, and an aqueous medium that could be distilled water or brine of specific salinity, to get accurate results using the DLVO model.

Zeta Potential (ζ). Zeta potential is an important indicator of surface charge and is used for the quantification of the electrostatic repulsive energy between dispersed fines and sand grains. It is the potential difference between the surfaces because of the electrical difference between a particle surface and points away from the particle in the fluid at the boundary of the slipping plane,[126,127] as shown in Figure 5. This potential is also known as electro-kinetic potential in colloidal dispersions. It is worth mentioning here that the measured zeta potential of clay particles (fines) is negative and is an important parameter that provides information about the charge on the particle surface, colloidal system stability in an ionic environment, electrostatic forces between particles and the rock surface, and interaction energy between NPs and formation fines in porous media. Zeta potential is an input parameter in the calculation of the EDL repulsive force and must be determined experimentally with great accuracy. It is usually measured with a Zetasizer, which uses the electrophoretic mobility (EFM) concept based on the Helmholtz Smoluchowski equation (shown in eq 16).

$$\zeta = \frac{U_E 3\eta}{2\varepsilon F(ka)} \quad (16)$$

Tables 7 and 8 present the zeta potential data collected from several previously published research articles that show the widespread use of this parameter. It is evident from the data that in all the studies, the zeta potential of the system has been determined with the help of the Zetasizer/zeta potential analyzer, which is a high-technology and expensive apparatus

https://dx.doi.org/10.1021/acsomega.0c03943
ACS Omega 2020, 5, 31624−31639

being used worldwide. It measures the electrophoretic mobility and automatically converts it to provide the direct zeta potential value of the system under study. No comprehensive correlation is available to directly calculate zeta potential as a function of system configuration (sand, glass beads, fines, kaolinite, calcite, etc.), salinity, viscosity, pH, and temperature.

Based on the data available in Table 8 for similar neutral systems (pH ≃ 7−8.5) containing sandstone and NaCl solutions of different I_s,[77,90,92,118,128] two correlations are developed to estimate zeta potential for high-salinity and low-salinity conditions, as shown in Figure 17. Equations 17 and 18 present the developed correlations for low-salinity (0−0.09 M) and high-salinity (0.1−0.9 M approx.) conditions, respectively.

$$\zeta\text{-potential (mV)} = 96.315 \times M - 38.786 + \text{error} \quad (17)$$

$$\zeta\text{-potential (mV)} = 25.658 \times M - 34.053 + \text{error} \quad (18)$$

These correlations are validated for specific salinity range with laboratory data taken from different studies with similar conditions (sandstone, pH ≃ 7−8.5, 25 °C). and the results are shown in Table 6. Model results are in close agreement with the laboratory measured zeta potential, with less than 10% error for most of the data points, as shown in Figure 18.

Hence, the generated models can be used to estimate the zeta potential of similar systems, eliminating the need to perform extensive experiments. The calculated zeta potential of sand grains demonstrates the contraction and expansion of the EDLs around fines and sand grains under different salinity conditions. Regarding the practical viewpoint, the developed correlations can considerably benefit the reservoir engineers and production chemists who are involved in the modeling and designing of injection water chemistry/recipe and operation in sandstone reservoirs to avoid fine migration while maintaining designed injectivity.

CONCLUSIONS

The DLVO modeling technique based on the quantification and analysis of surface forces is a powerful tool that helps in the analysis of fine migration and control in sandstone reservoirs during low-salinity water injection and alkaline flooding without extensive experimentation. The results can be summarized as follows:

(1) Based on surface force analysis of the FBR system for the solution containing monovalent and divalent ions, this tool can predict the CSC for the injection fluid below which the total interaction energy for the system becomes repulsive and the fine migration starts within the porous media.

(2) Attractive and repulsive forces are affected by fine particle size, ionic strength, types of ions, pH, and the viscosity of the flowing fluid, and all these factors must be considered for the quantification of surface forces.

(3) The application of NPs changes the surface energy and is a promising technique to control and optimize the fine migration with reduced critical salinity. Surface force analysis shows an increase in attractive interaction energy after the application of NPs.

(4) Zeta potential of the FBR system and Hamaker constant are important indicators for any change in attractive and repulsive forces. Precise measurements of these influential parameters can reduce uncertainty in the results and help to provide a better outcome.

AUTHOR INFORMATION

Corresponding Author

M. Rehan Hashmet − *School of Mining and Geosciences, Nazarbayev University, Nur-Sultan 010000, Kazakhstan;* orcid.org/0000-0001-9584-3307; Email: muhammad.hashmet@nu.edu.kz

Authors

Rizwan Muneer − *School of Mining and Geosciences, Nazarbayev University, Nur-Sultan 010000, Kazakhstan*

Peyman Pourafshary − *School of Mining and Geosciences, Nazarbayev University, Nur-Sultan 010000, Kazakhstan;* orcid.org/0000-0003-4600-6670

Complete contact information is available at: https://pubs.acs.org/10.1021/acsomega.0c03943

Notes

The authors declare no competing financial interest.

ACKNOWLEDGMENTS

The authors would like to thank Nazarbayev University for supporting this research through the NU Faculty Development Competitive Research Grants program (Application of Nanofluids to Control Formation Damage and Improved Oil Recovery Process, Code: 240919FD3928).

NOMENCLATURE

A_H, Hamaker constant, J
a_p, particle radius, nm
C, concentration of ion, M
e, electron charge, C = 1.60×10^{-19} C
$F(k_a)$, Henry's function
F_G, gravitational force, kg·m·s^{-2}
F_e, net electrostatic force, kg·m·s^{-2}
h, separation distance, nm
H, dimensionless distance = h/a_p
h_p, Planck constant, J s
I_s, ionic strength of permeating fluid, $=\frac{1}{2}\sum_{j=1}^{n} c_j z_j^2$
k_B, Boltzman constant, J K^{-1}
k, inverse Debye length, m^{-1} $=\sqrt{\frac{\epsilon k_B T}{2N_A e^2 I_s}}$
n, number of fines in a cluster
N_A, Avogadro's number = 6.02214×10^{23} mol^{-1}
R, average pore throat radius, m
T, absolute temperature, K
U_E, electrophoretic mobility, V
V_{LVW}, London−van der Waals potential
V_{EDL}, electrical double-layer potential
V_{BR}, Born repulsion potential
ν_e, electronic adsorption frequency, s^{-1}
z, valence of ion
v, flowing fluid velocity, m/s.
ϵ, dielectric constant in J^{-1} C^2 m^{-1}
ψ, potential, mV
η, refractive index
ζ, zeta potential, mV
σ, atomic collision diameter, nm
ϵ_m, relative static permittivity of water
ϵ_o, permittivity of the vacuum
η, viscosity of solution, kg m^{-1} s^{-1}
γ_s, $\tanh(ze\zeta_s/4k_BT)$
γ_g, $\tanh(ze\zeta_g/4k_BT)$

https://dx.doi.org/10.1021/acsomega.0c03943
ACS Omega 2020, 5, 31624−31639

REFERENCES

(1) Chavan, M.; Dandekar, A.; Patil, S.; Khataniar, S. Low-salinity-based enhanced oil recovery literature review and associated screening criteria. *Pet. Sci.* **2019**, *16*, 1344−1360.

(2) Austad, T.; RezaeiDoust, A.; Puntervold, T. Chemical mechanism of low salinity water flooding in sandstone reservoirs. *SPE Improved Oil Recovery Symposium*, 2010.

(3) Bjørlykke, K. *Petroleum Geoscience: From Sedimentary Environments to Rock Physics*; Springer: New York, 2015.

(4) Kaplan, D. A.; Muñoz-Carpena, R. Groundwater salinity in a floodplain forest impacted by saltwater intrusion. *J. Contam. Hydrol.* **2014**, *169*, 19−36.

(5) Mungan, N. Permeability reduction through changes in pH and salinity. *J. Pet. Technol.* **1965**, *17*, 1449−1453.

(6) McDowell-Boyer, L. M.; Hunt, J. R.; Sitar, N. Particle transport through porous media. *Water Resour. Res.* **1986**, *22*, 1901−1921.

(7) Sarkar, A. K.; Sharma, M. M. Fines migration in two-phase flow. *J. Pet. Technol.* **1990**, *42*, 646−652.

(8) Torkzaban, S.; Bradford, S. A.; Vanderzalm, J. L.; Patterson, B. M.; Harris, B.; Prommer, H. Colloid release and clogging in porous media: Effects of solution ionic strength and flow velocity. *J. Contam. Hydrol.* **2015**, *181*, 161−171.

(9) Chrysikopoulos, C. V.; Katzourakis, V. E. Colloid particle size-dependent dispersivity. *Water Resour. Res.* **2015**, *51*, 4668−4683.

(10) Sotirelis, N. P.; Chrysikopoulos, C. V. Heteroaggregation of graphene oxide nanoparticles and kaolinite colloids. *Sci. Total Environ.* **2017**, *579*, 736−744.

(11) Muecke, T. W. Formation fines and factors controlling their movement in porous media. *J. Pet. Technol.* **1979**, *31*, 144−150.

(12) Khilar, K. C.; Fogler, H. S. *Migrations of Fines in Porous Media*; Springer Science & Business Media: New Yor, 1998; Vol. *12*.

(13) Civan, F. *Reservoir Formation Damage-Fundamentals, Modeling, Assessment, and Mitigation*, 3rd ed.; Gulf Publishing Company: Houston, TX, 2016.

(14) Gomaa, I.; Mahmoud, M.; Kamal, M. S. Novel Approach for Sandstone Acidizing Using in Situ-Generated Hydrofluoric Acid with the Aid of Thermochemicals. *ACS Omega* **2020**, *5*, 1188−1197.

(15) Li, Z.; Du, C.; Tang, Y.; Li, X. Experimental and Statistical Investigation of Reservoir Properties with the Effect of Waterflooding Treatment. *ACS Omega* **2020**, *5*, 20922−20931.

(16) Morrow, N. R.; Tang, G.-q.; Valat, M.; Xie, X. Prospects of improved oil recovery related to wettability and brine composition. *J. Pet. Sci. Eng.* **1998**, *20*, 267−276.

(17) Ashraf, A.; Hadia, N.; Torsaeter, O.; Tweheyo, M. T. Laboratory investigation of low salinity waterflooding as secondary recovery process: effect of wettability. *SPE Oil and Gas India Conference and Exhibition*, 2010.

(18) Hassenkam, T.; Mitchell, A. C.; Pedersen, C. S.; Skovbjerg, L. L.; Bovet, N.; Stipp, S. L. S. The low salinity effect observed on sandstone model surfaces. *Colloids Surf., A* **2012**, *403*, 79−86.

(19) Collini, H.; Li, S.; Jackson, M. D.; Agenet, N.; Rashid, B.; Couves, J. Zeta potential in intact carbonates at reservoir conditions and its impact on oil recovery during controlled salinity waterflooding. *Fuel* **2020**, *266*, 116927.

(20) Takeya, M.; Shimokawara, M.; Elakneswaran, Y.; Nawa, T.; Takahashi, S. Predicting the electrokinetic properties of the crude oil/brine interface for enhanced oil recovery in low salinity water flooding. *Fuel* **2019**, *235*, 822−831.

(21) Mahani, H.; Menezes, R.; Berg, S.; Fadili, A.; Nasralla, R.; Voskov, D.; Joekar-Niasar, V. Insights into the impact of temperature on the wettability alteration by low salinity in carbonate rocks. *Energy Fuels* **2017**, *31*, 7839−7853.

(22) Kumar, M.; Fogden, A.; Morrow, N. R.; Buckley, J. S. Mechanisms of improved oil recovery from sandstone by low salinity flooding. *Petrophysics* **2011**, *52*, 428−436.

(23) Takeya, M.; Ubaidah, A.; Shimokawara, M.; Okano, H.; Nawa, T.; Elakneswaran, Y. Crude oil/brine/rock interface in low salinity waterflooding: Experiments, triple-layer surface complexation model, and DLVO theory. *J. Pet. Sci. Eng.* **2020**, *188*, 106913.

(24) Nasralla, R. A.; Alotaibi, M. B.; Nasr-El-Din, H. A. Efficiency of oil recovery by low salinity water flooding in sandstone reservoirs. *SPE Western North American Region Meeting*, 2011.

(25) Xie, Q.; Liu, Y.; Wu, J.; Liu, Q. Ions tuning water flooding experiments and interpretation by thermodynamics of wettability. *J. Pet. Sci. Eng.* **2014**, *124*, 350−358.

(26) Tang, G. Q.; Morrow, N. R. Salinity, temperature, oil composition, and oil recovery by waterflooding. *SPE Reservoir Eng.* **1997**, *12*, 269−276.

(27) Tang, G.-Q.; Morrow, N. R. Influence of brine composition and fines migration on crude oil/brine/rock interactions and oil recovery. *J. Pet. Sci. Eng.* **1999**, *24*, 99−111.

(28) Morrow, N.; Buckley, J. Improved oil recovery by low-salinity waterflooding. *J. Pet. Technol.* **2011**, *63*, 106−112.

(29) Lager, A.; Webb, K. J.; Black, C.; Singleton, M.; Sorbie, K. S. Low salinity oil recovery-an experimental investigation. *Petrophysics* **2008**, *49*, 28−35.

(30) Al-Sarihi, A.; Russell, T.; Bedrikovetsky, P.; Zeinijahromi, A. Fines Stabilization by Ca Ions and Its Effect on LSW Injection. *Energy Fuels* **2019**, *33*, 10775−10786.

(31) Yu, M.; Hussain, F.; Arns, J.-Y.; Bedrikovetsky, P.; Genolet, L.; Behr, A.; Kowollik, P.; Arns, C. H. Imaging analysis of fines migration during water flow with salinity alteration. *Adv. Water Resour.* **2018**, *121*, 150−161.

(32) Yu, M. An Experimental Investigation of Permeability Damage and Mobility Control During Fines-Assisted Waterflooding. Ph.D. Thesis, University of New South Wales, Sydney NSW 2052, Australia, 2018.

(33) Tangparitkul, S.; Saul, A.; Leelasukseree, C.; Yusuf, M.; Kalantariasl, A. Fines migration and permeability decline during reservoir depletion coupled with clay swelling due to low-salinity water injection: An analytical study. *J. Pet. Sci. Eng.* **2020**, *194*, 107448.

(34) Prempeh, K. O. K.; Chequer, L.; Badalyan, A.; Bedrikovetsky, P. Effects of the capillary-entrapped phase on fines migration in porous media. *J. Nat. Gas Sci. Eng.* **2020**, *73*, 103047.

(35) Yu, M.; Hussain, F.; Arns, J.-Y.; Bedrikovetsky, P.; Genolet, L.; Behr, A.; Kowollik, P.; Arns, C. H. Imaging analysis of fines migration during water flow with salinity alteration. *Adv. Water Resour.* **2018**, *121*, 150−161.

(36) Hussain, F.; Zeinijahromi, A.; Bedrikovetsky, P.; Badalyan, A.; Carageorgos, T.; Cinar, Y. An experimental study of improved oil recovery through fines-assisted waterflooding. *J. Pet. Sci. Eng.* **2013**, *109*, 187−197.

(37) Al-Sarihi, A.; Zeinijahromi, A.; Genolet, L.; Behr, A.; Kowollik, P.; Bedrikovetsky, P. Effects of fines migration on residual oil during low-salinity waterflooding. *Energy Fuels* **2018**, *32*, 8296−8309.

(38) Ahmetgareev, V.; Zeinijahromi, A.; Badalyan, A.; Khisamov, R.; Bedrikovetsky, P. Analysis of low salinity waterflooding in Bastrykskoye field. *Pet. Sci. Technol.* **2015**, *33*, 561−570.

(39) Izuwa, N. C.; Onwukwe, S. I.; Akinbamini, O. E. Evaluation of Fines Assisted Low Salinity Water Flooding in Edge Water Drive Reservoirs. *J. Pet. Environ. Biotechnol.* **2018**, *9*, 1000381.

(40) Yua, M.; Hussaina, F.; Bedrikovetskyb, P. Low-Salinity Waterflood with non-Polar Oil: the effects of fines migration excluding the wettability alteration effects. *International Symposium of the Society of Core Analysts*, 2017.

(41) Hussain, F.; Zeinijahromi, A.; Bedrikovetski, P.; Badalyan, A.; Carageorgos, T.; Cinar, Y. Enhanced oil recovery through low salinity fines-assisted waterflooding: laboratory and mathematical modelling. *SPE Asia Pacific Oil & Gas Conference and Exhibition*, 2014.

(42) Bedrikovetsky, P.; Zeinijahromi, A.; Badalyan, A.; Ahmetgareev, V.; Khisamov, R. Fines-Migration-Assisted Low-Salinity Waterflooding: Field Case Analysis (Russian). *SPE Russian petroleum technology conference*, 2015.

(43) Barkman, J. H.; Abrams, A.; Darley, H. C. H.; Hill, H. J. An Oil-Coating Process To Stabilize Clays in Fresh Waterflooding Operations-(includes associated paper 6405). *J. Pet. Technol.* **1975**, *27*, 1053−1059.

(44) Chrysikopoulos, C. V.; Masciopinto, C.; La Mantia, R.; Manariotis, I. D. Removal of biocolloids suspended in reclaimed

https://dx.doi.org/10.1021/acsomega.0c03943
ACS Omega 2020, 5, 31624−31639

wastewater by injection into a fractured aquifer model. *Environ. Sci. Technol.* **2010**, *44*, 971−977.
(45) Borazjani, S.; Chequer, L.; Russell, T.; Bedrikovetsky, P., Injectivity Decline During Waterflooding and PWRI due to Fines Migration. *SPE International Conference and Exhibition on Formation Damage Control*; Society of Petroleum Engineers: Lafayette: Louisiana, USA, 2018; p 11.
(46) You, Z.; Bedrikovetsky, P., Well Productivity Impairment Due to Fines Migration. *SPE International Conference and Exhibition on Formation Damage Control*; Society of Petroleum Engineers: Lafayette, Louisiana, USA, 2018; p 23.
(47) Asghari, K.; Kharrat, R.; Vossoughi, S., Alteration of Permeability by Fine Particle Movement - A Water Injectivity Problem. *SPE International Symposium on Oilfield Chemistry*; Society of Petroleum Engineers: San Antonio, Texas, 1995; p 11.
(48) Bennion, D. B. An Overview of Formation Damage Mechanisms Causing a Reduction in the Productivity and Injectivity of Oil and Gas Producing Formations. *J. Can. Pet. Technol.* **2002**, *41* (11), 29−36, DOI: DOI: 10.2118/02-11-DAS.
(49) Sharma, M. M.; Yortsos, Y. C. Transport of particulate suspensions in porous media: Model formulation. *AIChE J.* **1987**, *33*, 1636−1643.
(50) Al-Yaseri, A.; Zhang, Y.; Ghasemiziarani, M.; Sarmadivaleh, M.; Lebedev, M.; Roshan, H.; Iglauer, S. Permeability Evolution in Sandstone Due to CO2 Injection. *Energy Fuels* **2017**, *31*, 12390−12398.
(51) Othman, F.; Yu, M.; Kamali, F.; Hussain, F. Fines migration during supercritical CO2 injection in sandstone. *J. Nat. Gas Sci. Eng.* **2018**, *56*, 344−357.
(52) Wang, Q.; Yang, S.; Han, H.; Wang, L.; Qian, K.; Pang, J. Experimental investigation on the effects of CO2 displacement methods on petrophysical property changes of ultra-low permeability sandstone reservoirs near injection wells. *Energies* **2019**, *12*, 327.
(53) Sokama-Neuyam, Y. A.; Ginting, P. U. R.; Timilsina, B.; Ursin, J. R. The impact of fines mobilization on CO2 injectivity: an experimental study. *Int. J. Greenhouse Gas Control* **2017**, *65*, 195−202.
(54) Xie, Q.; Saeedi, A.; Delle Piane, C.; Esteban, L.; Brady, P. V. Fines migration during CO2 injection: Experimental results interpreted using surface forces. *Int. J. Greenhouse Gas Control* **2017**, *65*, 32−39.
(55) Sokama-Neuyam, Y. A.; Forsetløkken, S. L.; Lien, J.-e.; Ursin, J. R. The coupled effect of fines mobilization and salt precipitation on CO2 injectivity. *Energies* **2017**, *10*, 1125.
(56) Hibbeler, J.; Garcia, T.; Chavez, N. An integrated long-term solution for migratory fines damage. *SPE Latin American and Caribbean Petroleum Engineering Conference*, 2003.
(57) Al-Dahlan, M.; Nasr-El-Din, H.; Al-Qahtani, A. Evaluation of retarded HF acid systems. *SPE International Symposium on Oilfield Chemistry*, 2001.
(58) Kakadjian, S.; Zamora, F.; Venditto, J. J. Zeta potential altering system for increased fluid recovery, production, and fines control. *International Symposium on Oilfield Chemistry*, 2007.
(59) Valdya, R. N.; Fogler, H. S. Fines migration and formation damage: influence of pH and ion exchange. *SPE Prod. Eng.* **1992**, *7*, 325−330.
(60) Mansouri, M.; Nakhaee, A.; Pourafshary, P. Effect of SiO2 nanoparticles on fines stabilization during low salinity water flooding in sandstones. *J. Pet. Sci. Eng.* **2019**, *174*, 637−648.
(61) Díez, R.; Medina, O. E.; Giraldo, L. J.; Cortés, F. B.; Franco, C. A. Development of Nanofluids for the Inhibition of Formation Damage Caused by Fines Migration: Effect of the interaction of Quaternary Amine (CTAB) and MgO Nanoparticles. *Nanomaterials* **2020**, *10*, 928.
(62) Siddiqui, F. R.; Tso, C. Y.; Chan, K. C.; Fu, S. C.; Chao, C. Y. H. On trade-off for dispersion stability and thermal transport of Cu-Al2O3 hybrid nanofluid for various mixing ratios. *Int. J. Heat Mass Transfer* **2019**, *132*, 1200−1216.
(63) Kumar, R. S.; Sharma, T. Stable SiO2-TiO2 composite-based nanofluid of improved rheological behaviour for high-temperature oilfield applications. *Geosyst. Eng.* **2020**, *23*, 51−61.
(64) Alomair, O. A.; Matar, K. M.; Alsaeed, Y. H. Experimental study of enhanced-heavy-oil recovery in Berea sandstone cores by use of nanofluids applications. *SPE Reservoir Eval. Eng.* **2015**, *18*, 387−399.
(65) Arab, D.; Pourafshary, P. Nanoparticles-assisted surface charge modification of the porous medium to treat colloidal particles migration induced by low salinity water flooding. *Colloids Surf., A* **2013**, *436*, 803−814.
(66) Assef, Y.; Arab, D.; Pourafshary, P. Application of nanofluid to control fines migration to improve the performance of low salinity water flooding and alkaline flooding. *J. Pet. Sci. Eng.* **2014**, *124*, 331−340.
(67) Arab, D.; Pourafshary, P.; Ayatollahi, S.; Habibi, A. Remediation of colloid-facilitated contaminant transport in saturated porous media treated by nanoparticles. *Int. J. Environ. Sci. Technol.* **2014**, *11*, 207−216.
(68) Huang, T.; Crews, J. B.; Willingham, J. R.; Belcher, C. K. Nano-Sized Particles for Formation Fines Fixation. 2702936A1, 2012.
(69) Ahmadi, M.; Habibi, A.; Pourafshary, P.; Ayatollahi, S. An Experimental Study of Interaction between Nanoparticles' Deposition on a Sintered Porous Medium and Migratory Fines. *J. Porous Media* **2013**, *16*, 459−467.
(70) Franco, C. A.; Zabala, R.; Cortés, F. B. Nanotechnology applied to the enhancement of oil and gas productivity and recovery of Colombian fields. *J. Pet. Sci. Eng.* **2017**, *157*, 39−55.
(71) Habibi, A.; Ahmadi, M.; Pourafshary, P.; Ayatollahi, s.; Al-Wahaibi, Y. Reduction of fines migration by nanofluids injection: an experimental study. *SPE J.* **2012**, *18*, 309−318.
(72) Martin, J. C. The effects of clay on the displacement of heavy oil by water. *SPE Venezuelan Annual Meeting*, 1959.
(73) Khilar, K. C.; Fogler, H. S. The existence of a critical salt concentration for particle release. *J. Colloid Interface Sci.* **1984**, *101*, 214−224.
(74) Guo, Z.; Hussain, F.; Cinar, Y. Physical and analytical modelling of permeability damage in bituminous coal caused by fines migration during water production. *J. Nat. Gas Sci. Eng.* **2016**, *35*, 331−346.
(75) Fogden, A.; Kumar, M.; Morrow, N. R.; Buckley, J. S. Mobilization of fine particles during flooding of sandstones and possible relations to enhanced oil recovery. *Energy Fuels* **2011**, *25*, 1605−1616.
(76) Galal, S. K.; Elgibaly, A. A.; Elsayed, S. K. Formation damage due to fines migration and its remedial methods. *Egypt. J. Pet.* **2016**, *25*, 515−524.
(77) Hasannejad, R.; Pourafshary, P.; Vatani, A.; Sameni, A. Application of silica nanofluid to control initiation of fines migration. *Pet. Explor. Dev.* **2017**, *44*, 850−859.
(78) Khilar, K. C.; Vaidya, R. N.; Fogler, H. S. Colloidally-induced fines release in porous media. *J. Pet. Sci. Eng.* **1990**, *4*, 213−221.
(79) Gregory, J. Approximate expressions for retarded van der Waals interaction. *J. Colloid Interface Sci.* **1981**, *83*, 138−145.
(80) Israelachvili, J. N. Van der Waals forces between particles and surfaces. *Intermolecular and surface forces* 2011, *3*, 253-289. DOI: 10.1016/b978-0-12-375182-9.10013-2
(81) Mahmood, T.; Amirtharajah, A.; Sturm, T. W.; Dennett, K. E. A micromechanics approach for attachment and detachment of asymmetric colloidal particles. *Colloids Surf., A* **2001**, *177*, 99−110.
(82) Musharova, D.; Mohamed, I. M.; Nasr-El-Din, H. A. Detrimental effect of temperature on fines migration in sandstone formations. *SPE International Symposium and Exhibition on Formation Damage Control*, 2012.
(83) Mansa, R.; Ngassa Piegang, G. B.; Detellier, C. Kaolinite Aggregation in Book-Like Structures from Non-Aqueous Media. *Clays Clay Miner.* **2017**, *65*, 193−205.
(84) Żbik, M. S.; Raftery, N. A.; Smart, R. S. C.; Frost, R. L. Kaolinite platelet orientation for XRD and AFM applications. *Appl. Clay Sci.* **2010**, *50*, 299−304.
(85) Letaief, S.; Leclercq, J.; Liu, Y.; Detellier, C. Single Kaolinite Nanometer Layers Prepared by an In Situ Polymerization-Exfoliation Process in the Presence of Ionic Liquids. *Langmuir* **2011**, *27*, 15248−15254.

(86) Awad, M. E.; López-Galindo, A.; Setti, M.; El-Rahmany, M. M.; Iborra, C. V. Kaolinite in pharmaceutics and biomedicine. *Int. J. Pharm.* **2017**, *533*, 34−48.
(87) Samyn, P.; Schoukens, G.; Stanssens, D. Kaolinite Nanocomposite Platelets Synthesized by Intercalation and Imidization of Poly(styrene-co-maleic anhydride). *Materials* **2015**, *8*, 4363−4388.
(88) Habibi, A.; Heidari, M. A.; Al-Hadrami, H.; Al-Ajmi, A.; Al-Wahaibi, Y.; Ayatollahi, S. Effect of nanofluid treatment on water sensitive formation to investigate water shock phenomenon, an experimental study. *J. Dispersion Sci. Technol.* **2014**, *35*, 889−897.
(89) Yang, Y.; Siqueira, F. D.; Vaz, A. S. L.; You, Z.; Bedrikovetsky, P. Slow migration of detached fine particles over rock surface in porous media. *J. Nat. Gas Sci. Eng.* **2016**, *34*, 1159−1173.
(90) Chequer, L.; Bedrikovetsky, P.; Carageorgos, T.; Badalyan, A.; Gitis, V. Mobilization of Attached Clustered Colloids in Porous Media. *Water Resour. Res.* **2019**, *55*, 5696−5714.
(91) Huang, F.; Kang, Y.; You, L.; Li, X.; You, Z. Massive fines detachment induced by moving gas-water interfaces during early stage two-phase flow in coalbed methane reservoirs. *Fuel* **2018**, *222*, 193−206.
(92) Gomez-Flores, A.; Bradford, S. A.; Hwang, G.; Choi, S.; Tong, M.; Kim, H. Shape and orientation of bare silica particles influence their deposition under intermediate ionic strength: A study with QCM-D and DLVO theory. *Colloids Surf., A* **2020**, *599*, 124921.
(93) El-Monier, E. A.; Nasr-El-Din, H. A. Mitigation of fines migration using a new clay stabilizer: A mechanistic study. *SPE European Formation Damage Conference*, 2011.
(94) Sanaei, A.; Tavassoli, S.; Sepehrnoori, K. Investigation of modified Water chemistry for improved oil recovery: Application of DLVO theory and surface complexation model. *Colloids Surf., A* **2019**, *574*, 131−145.
(95) Jung, J.; Cao, S.; Al-Raoush, R.; Alshibli, K. Fines migration and clogging behavior in methane hydratebearing sediments. *Qatar Foundation Annual Research Conference Proceedings*; Hamad bin Khalifa University Press (HBKU Press), 2018; Vol. *2018*, Issue 1, p EEPD710.
(96) Jung, J.; Kang, H.; Cao, S. C.; Al-Raoush, R. I.; Alshibli, K.; Lee, J. Y. Effects of Fine-Grained Particles' Migration and Clogging in Porous Media on Gas Production from Hydrate-Bearing Sediments. *Geofluids* **2019**, *2019*, 5061216.
(97) Cao, S. C.; Jang, J.; Jung, J.; Waite, W. F.; Collett, T. S.; Kumar, P. 2D micromodel study of clogging behavior of fine-grained particles associated with gas hydrate production in NGHP-02 gas hydrate reservoir sediments. *Mar. Petrol. Geol.* **2019**, *108*, 714−730.
(98) Yuan, B.; Moghanloo, R. G. Analytical modeling nanoparticles-fines reactive transport in porous media saturated with mobile immiscible fluids. *AIChE J.* **2019**, *65*, No. e16702.
(99) Shuang, C.; Jung, J.; Kwon, T. The characteristics of fines migration and clogging of sediments recovered from the gas hydrate deposits from the Ulleng Basin, East sea, Korea. *Proceedings of the XVII ECSMGE*, 2019.
(100) Derjaguin, B.; Landau, L. The theory of stability of highly charged lyophobic sols and coalescence of highly charged particles in electrolyte solutions. *Acta Physicochim. URSS* **1941**, *14*, 58.
(101) Verwey, E. J. W. *Theory of the Stability of Lyophobic Colloids: The Interaction of Sol Particles Having an Electric Double Layer*; Elsevier, 1962, No. 541.3453 V4.
(102) Loeb, A. L.; Overbeek, J. T. G.; Wiersema, P. H.; King, C. V. The electrical double layer around a spherical colloid particle. *J. Electrochem. Soc.* **1961**, *108*, 269C.
(103) Zou, W.; Zhao, J.; Sun, C. Adsorption of Anionic Polyacrylamide onto Coal and Kaolinite Calculated from the Extended DLVO Theory Using the van Oss-Chaudhury-Good Theory. *Polymers* **2018**, *10*, 113.
(104) *Encyclopedic Dictionary of Polymers*; Gooch, J. W., Ed.; Springer; New York, 2010; p 582.
(105) Brewer, J.; Hunter, A. *Multimethod Research: A Synthesis of Styles*; Sage Publications, Inc, 1989.
(106) Elimelech, M.; Gregory, J.; Williams, R. *Particle Deposition and Aggregation*; Elsevier: Amsterdam, The Netherlands, 1995; pp 113−156.
(107) Evans, D. F.; Wennerstrom, H. *Colloidal Domain*; Wiley-Vch, 1999.
(108) Abramson, H.; Moyer, L.; Gorin, M. *Electrophoresis of Proteins*; Reinhold Publishing Corporation: New York, NY, 1942.
(109) Hogg, R.; Healy, T. W.; Fuerstenau, D. W. Mutual coagulation of colloidal dispersions. *Trans. Faraday Soc.* **1966**, *62*, 1638−1651.
(110) Gregory, J. Interaction of unequal double layers at constant charge. *J. Colloid Interface Sci.* **1975**, *51*, 44−51.
(111) Ruckenstein, E.; Prieve, D. C. Adsorption and desorption of particles and their chromatographic separation. *AIChE J.* **1976**, *22*, 276−283.
(112) Schumacher, G. A.; van de Ven, T. G. M. Brownian motion of charged colloidal particles surrounded by electric double layers. *Faraday Discuss. Chem. Soc.* **1987**, *83*, 75−85.
(113) Sahai, N. Is silica really an anomalous oxide? Surface acidity and aqueous hydrolysis revisited. *Environ. Sci. Technol.* **2002**, *36*, 445−452.
(114) Pate, K.; Safier, P. *Advances in Chemical Mechanical Planarization (CMP)*; Babu, S., Ed.; Woodhead Publishing: 2016; pp 299−325.
(115) Singh, R.; Mohanty, K. K. Nanoparticle-stabilized foams for high-temperature, high-salinity oil reservoirs. *SPE Annual Technical Conference and Exhibition*, 2017.
(116) Jeelani, P. G.; Mulay, P.; Venkat, R.; Ramalingam, C. Multifaceted Application of Silica Nanoparticles. A Review. *Silicon* **2020**, *12*, 1337−1354.
(117) Al-Anssari, S.; Arif, M.; Wang, S.; Barifcani, A.; Iglauer, S. Stabilising nanofluids in saline environments. *J. Colloid Interface Sci.* **2017**, *508*, 222−229.
(118) Xie, Q.; Saeedi, A.; Pooryousefy, E.; Liu, Y. Extended DLVO-based estimates of surface force in low salinity water flooding. *J. Mol. Liq.* **2016**, *221*, 658−665.
(119) Shehata, A. M.; Nasr-El-Din, H. A. Zeta potential measurements: Impact of salinity on sandstone minerals. *SPE International Symposium on Oilfield Chemistry*, 2015.
(120) Gulgonul, I. Zeta potential of Teflon in presence of monovalent and divalent ions. *Physicochem. Probl. Miner. Process.* **2019**, *55*, 792−801.
(121) Israelachvili, J. N. *Intermolecular and Surface Forces*. Elsevier Academic Press, 2015.
(122) El Badawy, A. M.; Scheckel, K. G.; Suidan, M.; Tolaymat, T. The impact of stabilization mechanism on the aggregation kinetics of silver nanoparticles. *Sci. Total Environ.* **2012**, *429*, 325−331.
(123) Peng, M.; Duignan, T. T.; Nguyen, A. V. Significant Effect of Surfactant Adsorption Layer Thickness in Equilibrium Foam Films. *J. Phys. Chem. B* **2020**, *124*, 5301−5310.
(124) Elimelech, M.; Gregory, J.; Jia, X.; Williams, R. Modelling of particle deposition onto ideal collectors. *Particle Deposition and Aggregation: Measurement, Modelling and Simulation*; Elsevier, 1995, pp 50005−50014.
(125) Xie, Q.; Chen, Y.; You, L.; Hossain, M.; Saeedi, A. Drivers of wettability alteration for oil/brine/kaolinite system: implications for hydraulic fracturing fluids uptake in shale rocks. *Energies* **2018**, *11*, 1666.
(126) Hunter, R. J. Principles and applications. *Zeta Potential in Colloid Science*; Academic Press: New York, 1981.
(127) Oldham, K. B. A Gouy-Chapman-Stern model of the double layer at a (metal)/(ionic liquid) interface. *J. Electroanal. Chem.* **2008**, *613*, 131−138.
(128) Nasralla, R. A.; Nasr-El-Din, H. A. Double-Layer Expansion: Is It A Primary Mechanism of Improved Oil Recovery by Low-Salinity Waterflooding?. *SPE Improved Oil Recovery Symposium*, 2012.
(129) Fogden, A. Effect of Water Salinity and pH on the Wettability of a Model Substrate. *Energy Fuels* **2011**, *25*, 5113−5125.
(130) Lebedeva, E. V.; Fogden, A. Micro-CT and wettability analysis of oil recovery from sand packs and the effect of waterflood salinity and kaolinite. *Energy Fuels* **2011**, *25*, 5683−5694.

https://dx.doi.org/10.1021/acsomega.0c03943
ACS Omega 2020, 5, 31624−31639

(131) Walker, E.; Glover, P. W. J. Measurements of the relationship between microstructure, pH, and the streaming and zeta potentials of sandstones. *Transp. Porous Media* **2018**, *121*, 183−206.
(132) Nguyen, V. S.; Rouxel, D.; Hadji, R.; Vincent, B.; Fort, Y. Effect of ultrasonication and dispersion stability on the cluster size of alumina nanoscale particles in aqueous solutions. *Ultrason. Sonochem.* **2011**, *18*, 382−388.
(133) Priya, K. R.; Suganthi, K.; Rajan, K. Transport properties of ultra-low concentration CuO−water nanofluids containing non-spherical nanoparticles. *Int. J. Heat Mass Transfer* **2012**, *55*, 4734−4743.
(134) Suganthi, K. S.; Rajan, K. S. Temperature induced changes in ZnO-water nanofluid: Zeta potential, size distribution and viscosity profiles. *Int. J. Heat Mass Transfer* **2012**, *55*, 7969−7980.
(135) Bayat, A. E.; Junin, R.; Shamshirband, S.; Chong, W. T. Transport and retention of engineered Al_2O_3, TiO_2, and SiO_2 nanoparticles through various sedimentary rocks. *Sci. Rep.* **2015**, *5*, 14264.
(136) Sabiha, M. A.; Mostafizur, R. M.; Saidur, R.; Mekhilef, S. Experimental investigation on thermo physical properties of single walled carbon nanotube nanofluids. *Int. J. Heat Mass Transfer* **2016**, *93*, 862−871.
(137) Adil, M.; Zaid, H. M.; Chuan, L. K.; Latiff, N. R. A. Effect of dispersion stability on electrorheology of water-based ZnO nanofluids. *Energy Fuels* **2016**, *30*, 6169−6177.
(138) Lee, J.; Moesari, E.; Dandamudi, C. B.; Beniah, G.; Chang, B.; Iqbal, M.; Fei, Y.; Zhou, N.; Ellison, C. J.; Johnston, K. P. Behavior of Spherical Poly(2-acrylamido-2-methylpropanesulfonate) Polyelectrolyte Brushes on Silica Nanoparticles up to Extreme Salinity with Weak Divalent Cation Binding at Ambient and High Temperature. *Macromolecules* **2017**, *50*, 7699−7711.
(139) Abdelfatah, E.; Kang, K.; Pournik, M.; Shiau, B.; Harwell, J.; Haroun, M.; Rahman, M. Study of nanoparticle adsorption and release in porous media based on the DLVO theory. *SPE Latin America and Caribbean Petroleum Engineering Conference*, 2017.
(140) Skoglund, S.; Blomberg, E.; Wallinder, I. O.; Grillo, I.; Pedersen, J. S.; Bergström, L. M. A novel explanation for the enhanced colloidal stability of silver nanoparticles in the presence of an oppositely charged surfactant. *Phys. Chem. Chem. Phys.* **2017**, *19*, 28037−28043.
(141) Choudhary, R.; Khurana, D.; Kumar, A.; Subudhi, S. Stability analysis of Al2O3/water nanofluids. *J. Exp. Nanosci.* **2017**, *12*, 140−151.
(142) Upendar, S.; Mani, E.; Basavaraj, M. G. Aggregation and stabilization of colloidal spheroids by oppositely charged spherical nanoparticles. *Langmuir* **2018**, *34*, 6511−6521.
(143) Kuang, W.; Saraji, S.; Piri, M. A systematic experimental investigation on the synergistic effects of aqueous nanofluids on interfacial properties and their implications for enhanced oil recovery. *Fuel* **2018**, *220*, 849−870.
(144) Ma, L.; Luo, P.; He, Y.; Zhang, L.; Fan, Y.; Jiang, Z. Ultra-Stable Silica Nanoparticles as Nano-Plugging Additive for Shale Exploitation in Harsh Environments. *Nanomaterials* **2019**, *9*, 1683.
(145) Siddiqui, F. R.; Tso, C. Y.; Chan, K. C.; Fu, S. C.; Chao, C. Y. H. Dataset on critical parameters of dispersion stability of Cu/Al2O3 nanofluid and hybrid nanofluid for various ultra-sonication times. *Data Brief* **2019**, *22*, 863−865.
(146) Aramendiz, J.; Imqam, A. Water-based drilling fluid formulation using silica and graphene nanoparticles for unconventional shale applications. *J. Pet. Sci. Eng.* **2019**, *179*, 742−749.
(147) Wang, Z.; Babadagli, T.; Maeda, N. Preliminary Screening and Formulation of New Generation Nanoparticles for Stable Pickering Emulsion in Cold and Hot Heavy-Oil Recovery. *SPE Reservoir Eval. Eng.* **2020**, *14*, DOI: DOI: 10.2118/200190-PA.
(148) Yousef, A. A.; Al-Saleh, S.; Al-Jawfi, M. S. The impact of the injection water chemistry on oil recovery from carbonate reservoirs. *SPE EOR Conference at Oil and Gas West Asia*, 2012.
(149) Chen, L.; Zhang, G.; Wang, L.; Wu, W.; Ge, J. Zeta potential of limestone in a large range of salinity. *Colloids Surf., A* **2014**, *450*, 1−8.
(150) Yao, J.; Han, H.; Hou, Y.; Gong, E.; Yin, W. A method of calculating the interaction energy between particles in minerals flotation. *Math. Probl. Eng.* **2016**, *2016*, 8430745.
(151) Alghamdi, A.; Ayirala, S.; Alotaibi, M.; Alyousef, A. Electro-Kinetic Induced Wettability Alteration for Enhanced Oil Recovery in Carbonates. *International Petroleum Technology Conference*, 2020.
(152) Ruan, B.; Wu, P.; Liu, J.; Jiang, L.; Wang, H.; Qiao, J.; Zhu, N.; Dang, Z.; Luo, H.; Yi, X. Adhesion of Sphingomonas sp. GY2B onto montmorillonite: A combination study by thermodynamics and the extended DLVO theory. *Colloids Surf., B* **2020**, *192*, 111085.

https://dx.doi.org/10.1021/acsomega.0c03943
ACS Omega 2020, 5, 31624−31639